

Article

# Single and Dual Metal Oxides as Promising Supports for Carbon Monoxide Removal from an Actual Syngas: The Crucial Role of Support on the Selectivity of the Au–Cu System

Bernay Cifuentes <sup>1</sup>, Felipe Bustamante <sup>2</sup> and Martha Cobo <sup>1,\*</sup>

<sup>1</sup> Energy, Materials, and Environment Laboratory, Chemical Engineering Department, Universidad de La Sabana, Campus Universitario Puente del Común, Km. 7 Autopista Norte, Bogotá 250001, Colombia; bernay.cifuentes1@unisabana.edu.co

<sup>2</sup> Environmental Catalysis Research Group, Chemical Engineering Department, Universidad de Antioquia UdeA, Calle 70 No. 52-21, Medellín 050010, Colombia; felipe.bustamante@udea.edu.co

\* Correspondence: martha.cobo@unisabana.edu.co; Tel.: +571-8615555 (ext. 25207); Fax: +571-8615555

Received: 9 September 2019; Accepted: 10 October 2019; Published: 13 October 2019



**Abstract:** A catalytic screening was performed to determine the effect of the support on the performance of an Au–Cu based system for the removal of CO from an actual syngas. First, a syngas was obtained from reforming of ethanol. Then, the reformer outlet was connected to a second reactor, where Au–Cu catalysts supported on several single and dual metal oxides (i.e., CeO<sub>2</sub>, SiO<sub>2</sub>, ZrO<sub>2</sub>, Al<sub>2</sub>O<sub>3</sub>, La<sub>2</sub>O<sub>3</sub>, Fe<sub>2</sub>O<sub>3</sub>, CeO<sub>2</sub>-SiO<sub>2</sub>, CeO<sub>2</sub>-ZrO<sub>2</sub>, and CeO<sub>2</sub>-Al<sub>2</sub>O<sub>3</sub>) were evaluated. AuCu/CeO<sub>2</sub> was the most active catalyst due to an elevated oxygen mobility over the surface, promoting CO<sub>2</sub> formation from adsorption of C–O\* and OH<sup>−</sup> intermediates on Au<sup>0</sup> and CuO species. However, its lower capacity to release the surface oxygen contributes to the generation of stable carbon deposits, which lead to its rapid deactivation. On the other hand, AuCu/CeO<sub>2</sub>-SiO<sub>2</sub> was more stable due to its high surface area and lower formation of formate and carbonate intermediates, mitigating carbon deposits. Therefore, use of dual supports could be a promising strategy to overcome the low stability of AuCu/CeO<sub>2</sub>. The results of this research are a contribution to integrated production and purification of H<sub>2</sub> in a compact system.

**Keywords:** CO-PROX; CO-SMET; CO<sub>2</sub> methanation; hydrogen purification; process integration

## 1. Introduction

Synthesis gas (syngas) is used as a chemical building block in the synthesis of commodity chemicals and for energy applications. Specifically, syngas can be used in combustion processes [1], gas turbines [2], or hydrogen fuel cells (H<sub>2</sub>-FC) [3] to produce energy. The H<sub>2</sub>-FC are promising systems to provide sustainable energy for households, industry, transportation, and small devices. Likewise, the use of H<sub>2</sub>-FC has been proposed as an alternative to supply energy in places that are not connected to the electrical network and for remote installations [4].

The syngas composition varies depending on the production source, but mostly contains H<sub>2</sub>, carbon monoxide (CO), and light hydrocarbons. Bioethanol reforming is one of the most used pathways to produce syngas due to its high yield to H<sub>2</sub> [5]. In a previous study [6], we obtained a syngas containing H<sub>2</sub>, CO, CO<sub>2</sub>, CH<sub>4</sub>, and H<sub>2</sub>O from ethanol steam reforming (ESR) using a RhPt/CeO<sub>2</sub>-SiO<sub>2</sub> catalyst. Syngas production remained stable for 72 h of continuous operation and on/off cycles. This syngas could be used for sustainable energy production in H<sub>2</sub>-FC. However, CO must be removed from the syngas because of its harmful effect on fuel cell electrodes [7].

One of the most used strategies of CO removal from syngas is via chemical pathways, which includes preferential oxidation of CO (CO-PROX) [8,9], water gas shift reaction (WGS) [10], and selective CO methanation (CO-SMET) [10]. Traditionally, the objective of the CO cleanup step is to ensure CO concentrations below 10 ppm, which requires several catalytic reactors in series [11] and presents a high operating cost. However, recent research studies have allowed the development of H<sub>2</sub>-FC systems that tolerate CO concentrations above 100 ppm [12–14]. These contributions facilitate the use of less complex systems for syngas purification, which could lead to the development of more compact and economic H<sub>2</sub> technology.

Anticipating the commercialization of a new generation of more CO-tolerant H<sub>2</sub>-FC, it has been proposed to redesign the CO removal stage to reduce the number of process units in syngas purification. The new approach seeks to carry out CO removal using a single catalytic reactor, where several reactions occur simultaneously (i.e., CO-PROX, WGS, and CO-SMET). Kugai et al. [15] studied Pt–Cu and Pd–Cu bimetallic catalysts supported on CeO<sub>2</sub> for oxygen-enhanced water gas shift (OWGS), where WGS and CO-PROX occur concurrently, reporting higher CO removal from a model reformat gas (synthetic syngas) in the OWGS compared to the WGS carried out individually. Similarly, Xu and Zhang [16] reported that the presence of CO-SMET during CO-PROX on a commercial Ru/Al<sub>2</sub>O<sub>3</sub> catalyst allows for wider temperature windows that ensure the CO removal of a synthetic syngas. Despite these valuable contributions, the CO removal from syngas in a compact system is still at laboratory scale. Among the limitations for evaluation at the pilot scale is the lack of consensus regarding the catalyst and the most appropriate operating conditions to carry out the syngas purification.

Au is recognized as a promising catalyst in the three cleaning reactions of syngas (i.e., CO-PROX, WGS, and CO-SMET) [17,18]. Reina et al. [19] evaluated bimetallic catalysts of Au–M (M = La, Ni, Cu, Fe, Cr, Y), reporting that CO oxidation is favored by the Au–Cu combination because Cu interacts strongly with the support, favoring the oxygen mobility in the catalyst. Also, in a previous study [20], we evaluated Au–Cu bimetallic catalysts supported on CeO<sub>2</sub> for CO removal from a syngas obtained from ESR. It was possible to reduce the CO concentration below 100 ppm, but the catalyst showed rapid deactivation after 40 h. Deactivation was related to structural changes in the support and to the accumulation of carbonaceous compounds during continuous operation. Thus, this study illustrated that the support plays a key role in CO removal from an actual syngas, and led us to evaluate different supports for CO removal from a syngas in the search for a stable material.

Figure 1 shows the supports most used in the CO removal processes (i.e., WGS, CO-PROX, CO-SMET, or their combinations). CeO<sub>2</sub>, Fe<sub>2</sub>O<sub>3</sub>, ZrO<sub>2</sub>, TiO<sub>2</sub>, and Al<sub>2</sub>O<sub>3</sub> are the most commonly used single supports in CO removal from synthetic syngas. However, there is a growing interest in mixed supports (dual metal oxides), because they may have characteristics not observed in individual supports [21]. Most combinations of dual metal oxides include CeO<sub>2</sub> in the matrix, usually combined with supports that provide larger surface area, such as Al<sub>2</sub>O<sub>3</sub> [22] and SiO<sub>2</sub> [23], or with basic oxides, such as ZrO<sub>2</sub>, to generate new active sites [24]. TiO<sub>2</sub> is mainly used in CO removal by photocatalytic processes [25] and was not considered in this study. On the other hand, although La<sub>2</sub>O<sub>3</sub> is not among the most used supports in CO removal, it was recently reported that La<sub>2</sub>O<sub>3</sub> is effective for avoiding carbon deposits during CO-SMET [26].

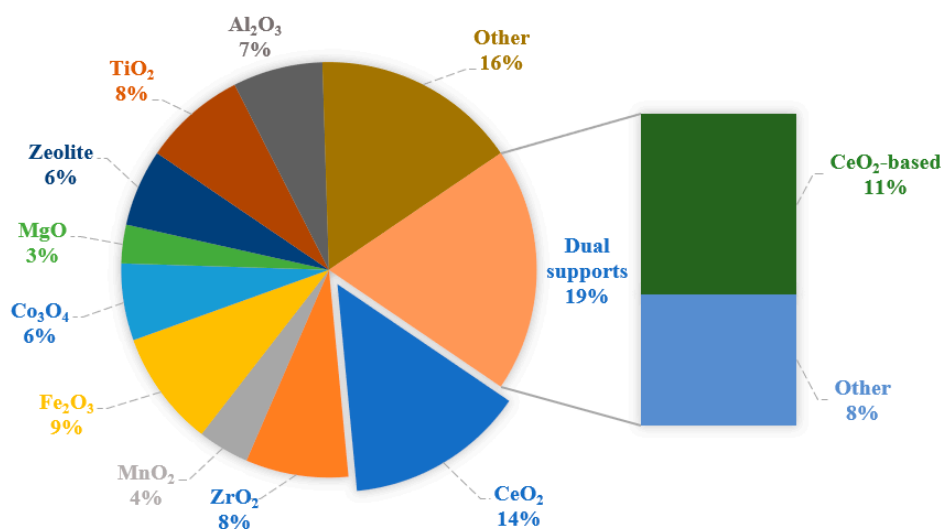


**Figure 1.** Supports used in CO removal from syngas streams using CO-PROX, WGSR or CO-SMET reactions.

Although several supports for syngas cleanup have been proposed, each investigation was carried out under different experimental conditions and using synthetic syngas, which makes it difficult to select the most suitable support for the CO removal. Therefore, the objective of this work was to study the CO removal from an actual syngas using bimetallic catalysts of AuCu-supported on single and dual metal oxides. Specifically, CeO<sub>2</sub>, ZrO<sub>2</sub>, La<sub>2</sub>O<sub>3</sub>, Fe<sub>2</sub>O<sub>3</sub>, Al<sub>2</sub>O<sub>3</sub>, and SiO<sub>2</sub> were selected as single metal oxides, and CeO<sub>2</sub>-SiO<sub>2</sub>, CeO<sub>2</sub>-ZrO<sub>2</sub>, and CeO<sub>2</sub>-Al<sub>2</sub>O<sub>3</sub> as dual metal oxides. The catalytic performance of the supports with and without active metals (i.e., Au and Cu) was evaluated. Then, the activity, selectivity, and stability were established as criteria for selecting the most suitable support for the CO elimination. In addition, characterization tests were conducted, such as temperature programmed reduction (TPR), surface area tests using the Brunauer-Emmett-Teller (BET) method, oxygen storage capacity (OSC) tests, thermogravimetric analysis (TGA), and in situ diffuse reflectance infrared Fourier transform spectroscopy (DRIFTS).

## 2. Results and Discussion

### 2.1. Activity, Selectivity, and Stability

Figure 2 shows the CO conversion in the cleanup reactor on the bare supports (i.e., without Au and Cu) and Au–Cu-supported catalysts. CeO<sub>2</sub> and ZrO<sub>2</sub> display the larger CO conversion between single metal oxides (Figure 2a). Indeed, the presence of oxygen vacancies on the surface of an oxide could favor a support showing high activity in the CO oxidation, despite the absence of active metals [27]; on the other hand, supports with low OSC, such as Al<sub>2</sub>O<sub>3</sub> [28], present lower activity. The use of dual metal oxides has been proposed as a strategy to overcome the deficiencies of single supports [21]. Figure 2b shows that CeO<sub>2</sub>-SiO<sub>2</sub> increases the CO conversion compared to SiO<sub>2</sub>, which could be associated with the interaction between the two oxides. However, no significant improvement in the CO conversion with CeO<sub>2</sub>-Al<sub>2</sub>O<sub>3</sub> was observed, and even for CeO<sub>2</sub>-ZrO<sub>2</sub>, the combination of the two metal oxides leads to a less active material. Furthermore, below 260 °C the dual metal oxides showed less activity than single CeO<sub>2</sub>, suggesting that the combination of several metal oxides does not always lead to more active materials in the syngas cleaning.

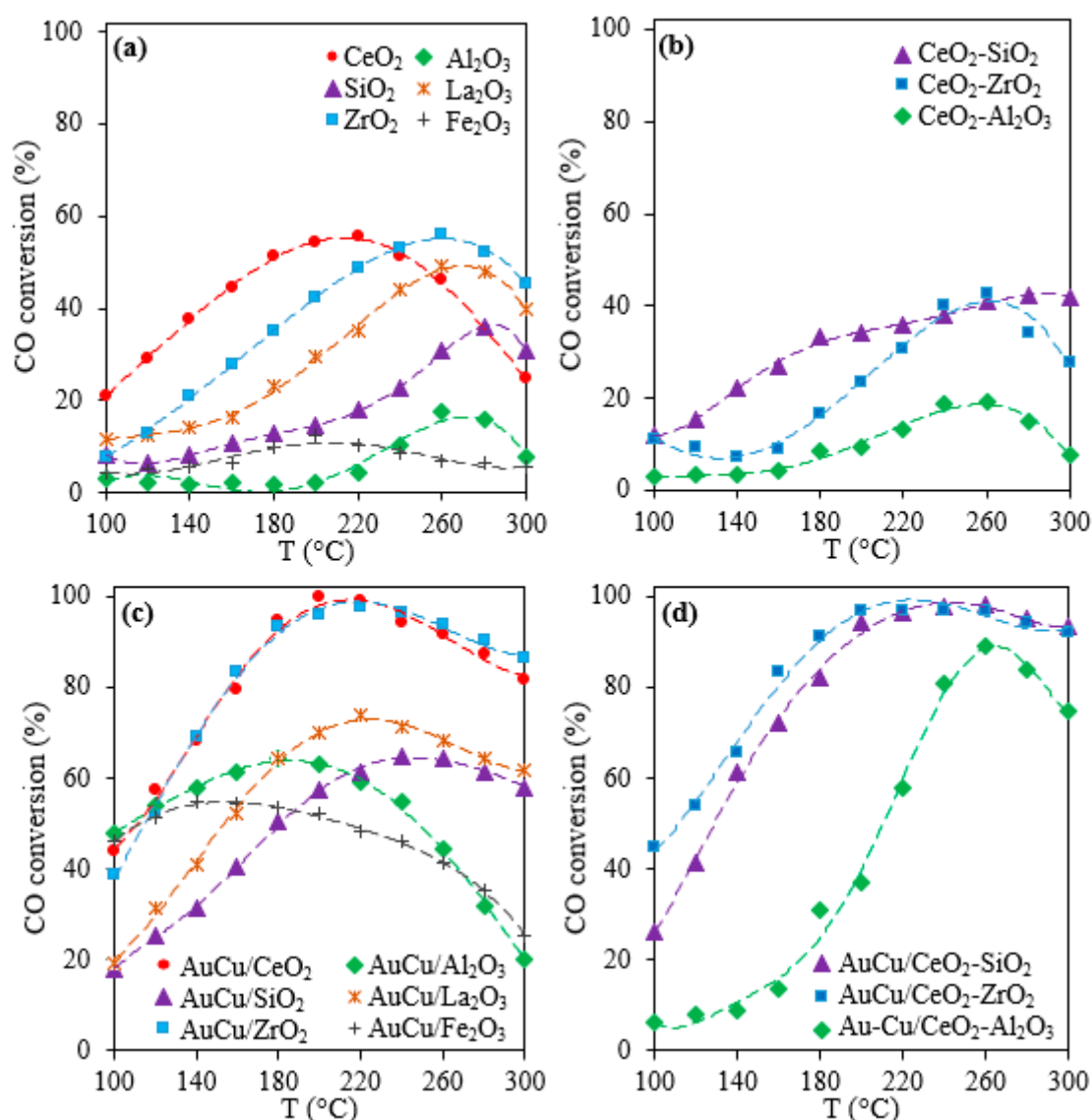


**Figure 2.** CO conversion obtained in the Cleanup reactor with supports (a,b) and supported 1 wt% Au–1 wt% Cu catalysts (c,d). Syngas feed: 7.8% H<sub>2</sub>, 2.0% CO, 0.5% CO<sub>2</sub>, 0.3% CH<sub>4</sub>, 1.4% H<sub>2</sub>O, 1.8% O<sub>2</sub>, 6.8% N<sub>2</sub>, and 79.4% Ar. Reaction conditions: Space velocity (SV) = 6.5 ± 0.2 L/g<sub>cat</sub>\*min and 0.3 g of the catalytic bed.

On the other hand, catalytic systems based on Au, Cu and Au–Cu have been studied extensively for the CO oxidation, CO-PROX, WGS, and CO-SMET. In-depth descriptions for Cu/CeO<sub>2</sub> [9], AuCu/CeO<sub>2</sub> [29], AuCu/SiO<sub>2</sub> [30], AuCu/Al<sub>2</sub>O<sub>3</sub> [31], Au/Fe<sub>2</sub>O<sub>3</sub> [32], Au/La<sub>2</sub>O<sub>3</sub>/Al<sub>2</sub>O<sub>3</sub> [33], and Au/CeO<sub>2</sub>-ZrO<sub>2</sub> [34,35] are available in the literature. In general, Au favors the CO conversion through a mechanism that involves Au–CO and Au–OOH species [36], where the formation of C–O\* intermediates determines the selectivity of the process [20], while CuO acts through a redox mechanism [8], promoting oxygen mobility in the oxide lattice [37] and facilitating the CO oxidation. A synergistic Au–Cu effect has also been proposed [19,29,38]. Therefore, the inclusion of 1 wt% Au and 1 wt% Cu in the single and dual metal oxides promotes greater CO conversion (Figure 2). Despite having the same active metals (i.e., Au and Cu), the catalysts showed maximum CO conversion at different temperatures, indicating that the properties of the support have a key role in the syngas cleaning. Table 1 shows that only AuCu/CeO<sub>2</sub> reached CO concentrations below 100 ppm in the actual syngas at 210 °C, whereas minimum CO concentrations of the other catalysts were above 500 ppm.

**Table 1.** Minimum concentration of CO obtained in syngas, apparent active metal dispersion (H/M ratio), surface area, OSC, and OSCC of Au–Cu catalysts supported on single and dual supports.

Catalyst <sup>a</sup>	Minimum CO Concentration in Outlet Gas (ppm) <sup>b</sup>	H/M Index	BET Surface Area (m <sup>2</sup> /g <sub>cat</sub> )		OSC in AC Samples (μmol O <sub>2</sub> /g <sub>cat</sub> )		OSCC at 300 °C (μmol O <sub>2</sub> /g <sub>cat</sub> )	
			AC	Spent	100 °C	300 °C	Fresh	Spent
AuCu/CeO <sub>2</sub>	75 at 210 °C	0.9	60	58 (U) 50 (S)	41	91	230	121 (U) 93 (S)
AuCu/SiO <sub>2</sub>	8320 at 240 °C	0.7	364	277 (U)	21	37	45	41 (U)
AuCu/ZrO <sub>2</sub>	507 at 225 °C	0.8	58	47 (U)	39	76	185	84 (U)
AuCu/Al <sub>2</sub> O <sub>3</sub>	745 at 180 °C	0.8	90	65 (U)	31	35	75	41 (U)
AuCu/La <sub>2</sub> O <sub>3</sub>	5365 at 225 °C	0.4	19	18 (U)	21	41	90	24 (U)
AuCu/Fe <sub>2</sub> O <sub>3</sub>	9416 at 140 °C	0.4	16	5 (U)	NR	NR	NR	NR
AuCu/CeO <sub>2</sub> -SiO <sub>2</sub>	861 at 230 °C	1.6	110	75 (U) 74 (S)	34	78	146	121 (U) 126 (S)
AuCu/CeO <sub>2</sub> -ZrO <sub>2</sub>	941 at 210 °C	0.9	42	30 (U)	42	94	210	162 (U)
AuCu/CeO <sub>2</sub> -Al <sub>2</sub> O <sub>3</sub>	1521 at 260 °C	1.2	65	56 (U)	32	79	155	121 (U)

<sup>a</sup> Nominal metal loadings: 1 wt% Au and 1 wt% Cu. <sup>b</sup> Value includes the carrier gas. AC: activated catalyst, which were reduced with H<sub>2</sub> and stabilized in air before activity tests. U: sample used to obtain light-off curves. S: sample evaluated in the stability test. Note: NR = Not reported; OSC = oxygen storage capacity; OSCC = oxygen storage complete capacity; BET: Brunauer-Emmett-Teller test.

On the other hand, the selectivity in the CO removal has been attributed to the support rather than the active metal [39], being the consumption of H<sub>2</sub> an important criterion in catalyst selection [39]. Figure 3 shows that H<sub>2</sub> consumption increases with temperature, particularly in the supports and catalysts based on ZrO<sub>2</sub>. The deficiency of ZrO<sub>2</sub> to adsorb/desorb bidentate carbonates above 150 °C has been associated with a promotion of the H<sub>2</sub> combustion over the CO oxidation [40]. Likewise, H<sub>2</sub> loss increases in the majority of the supported Au–Cu catalysts (Figure 3c,d) compared to their respective bare support (Figure 3a,b), possibly due to affinity of the Au–Cu system to form intermediates in the H<sub>2</sub> oxidation (e.g., hydroxyl groups [29,41]) and methane formation (e.g., C–O\* species [18,20,42]). Also, the most active catalysts in the CO removal (i.e., AuCu/CeO<sub>2</sub>, AuCu/ZrO<sub>2</sub>, AuCu/CeO<sub>2</sub>-SiO<sub>2</sub>, and AuCu/CeO<sub>2</sub>-ZrO<sub>2</sub>) promote higher H<sub>2</sub> consumption. That is, an active catalyst in the CO conversion possibly has an inherent tendency to consume H<sub>2</sub>. The high H<sub>2</sub> consumption, which in some cases exceeds 20%, could be associated with the syngas composition [20,37], specifically with the H<sub>2</sub>/CO ratio. Table 2 shows the results obtained in the CO removal with catalytic systems based on Au–Cu. High H<sub>2</sub>/CO ratios (>>10 [43]) are used in CO-PROX with synthetic syngas to favor CO oxidation [44] and reduce the H<sub>2</sub> consumption. To achieve such high H<sub>2</sub>/CO ratios before CO-PROX several WGS reactors are required, however [11]. Thence, aiming at reducing the number of units used in the traditional process, it has been proposed to carry out CO removal reactions in a single reactor using the syngas that comes directly from the reformer [15,20,35]. Nevertheless, the syngas obtained directly from the ESR contains larger amounts of CO. H<sub>2</sub>/CO ratios around 4 have been reported for syngas obtained from ESR using Ir/CeO<sub>2</sub> [45] and RhPd/CeO<sub>2</sub> [46] catalysts. Thus, the low H<sub>2</sub>/CO ratio in the actual syngas (e.g., the syngas used in this work has an H<sub>2</sub>/CO = 4) could conduce to a high H<sub>2</sub> loss in the cleanup reactor. Simultaneous production of CO<sub>2</sub> and CH<sub>4</sub> was observed in all catalysts evaluated (Figures A1 and A2 in Appendix A), suggesting that CO-SMET and CO<sub>2</sub> methanation occur together with CO-PROX and WGS. Then, H<sub>2</sub> oxidation and carbon hydrogenation would be the main causes of H<sub>2</sub> loss during the CO removal from an actual syngas.

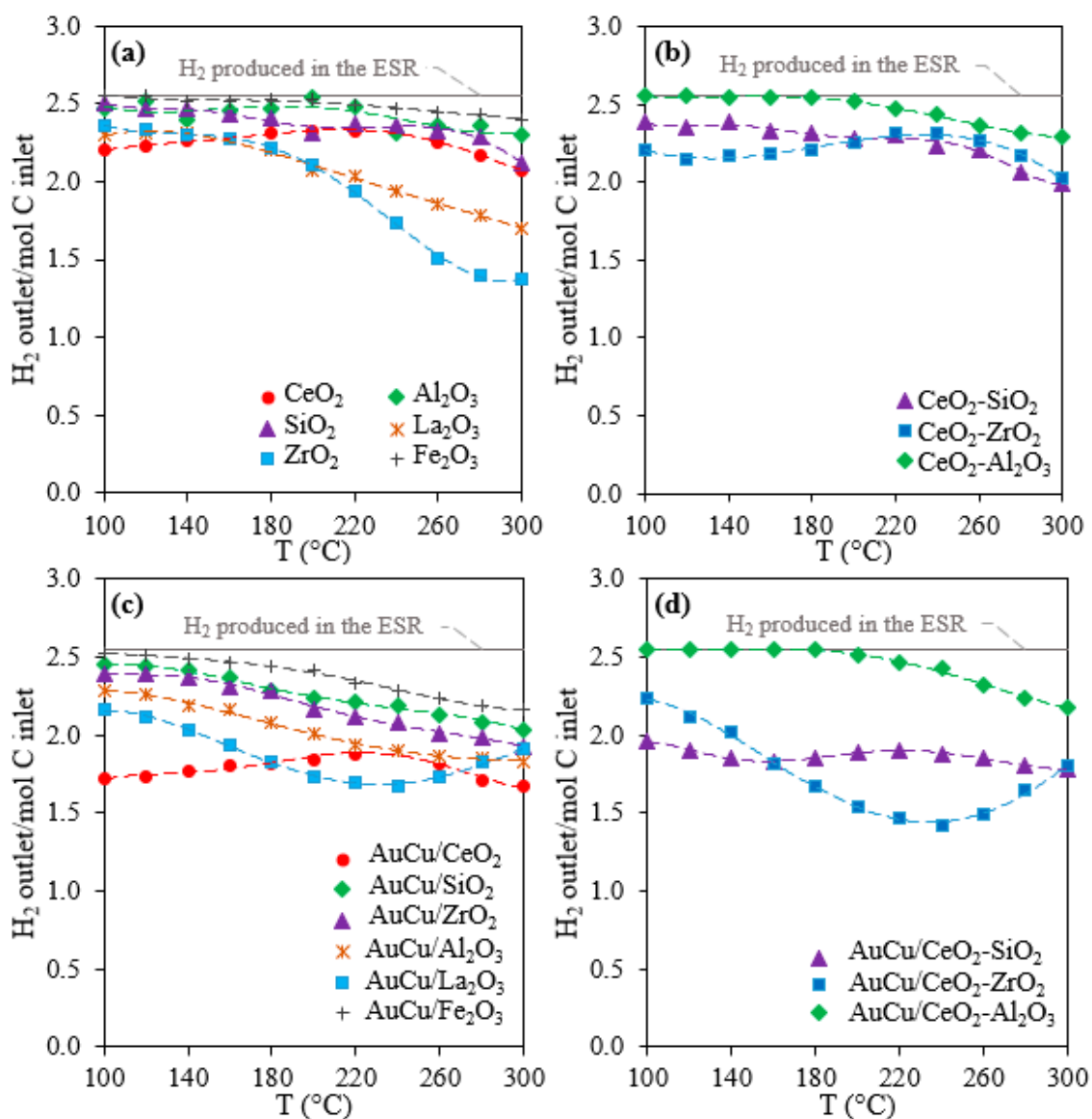


**Figure 3.** H<sub>2</sub> yield obtained from a system that integrate the ethanol steam reforming (ESR) reactor and the cleanup reactor, where the CO removal is performed with bare supports (a,b) and supported 1 wt% Au–1 wt% Cu catalysts (c,d). Reaction conditions: SV = 6.5 ± 0.2 L/g<sub>cat</sub>\*min and 0.3 g of the catalytic bed in both reactors.

**Table 2.** Comparison of various catalytic systems for the CO removal using Au–Cu catalysts.

Catalyst	Syngas Type	H <sub>2</sub> /CO	T (°C)	CO Conversion (%)	H <sub>2</sub> Loss (%)	Ref.
AuCu/CeO <sub>2</sub>	Synthetic	30	220	90	2	[29]
AuCu/SBA-15	Synthetic	>50	25	100	5 <sup>a</sup>	[47]
Au/CuO-CeO <sub>2</sub> /Al <sub>2</sub> O <sub>3</sub>	Synthetic	4.5	350	75	NR	[17]
Au/CeO <sub>2</sub> -CuO <sub>2</sub> /Al <sub>2</sub> O <sub>3</sub>	Synthetic	50	110	95	3 <sup>a</sup>	[19]
Au/Al <sub>2</sub> O <sub>3</sub>	Synthetic	>50	80	99	2 <sup>a</sup>	[36]
Au/CeO <sub>2</sub> -ZrO <sub>2</sub>	Actual	30	100	99	2 <sup>a</sup>	[35]
AuCu/CeO <sub>2</sub>	Actual	4	210	99	17	This work
AuCu/CeO <sub>2</sub> -SiO <sub>2</sub>	Actual	4	230	97	19	This work

<sup>a</sup> Calculated by O<sub>2</sub> mass balance. NR: Not reported.

Although  $\text{CH}_4$  formation implicitly involves an undesirable  $\text{H}_2$  consumption, it has been reported that a combination of CO-PROX and methanation improves CO removal compared to the CO-PROX alone, because of favoritism in the activation of adsorbed CO [16]. Then, C and H mass balances were carried out to determine the effect of  $\text{CH}_4$  production on  $\text{H}_2$  consumption and CO conversion. Figure 4 shows the  $\text{H}_2$  and CO converted with respect to the  $\text{CH}_4$  formed in the cleanup reactor.  $\text{CH}_4$  formation appears to be directly proportional to  $\text{H}_2$  loss (Figure 4a), but the amount of  $\text{H}_2$  consumed is larger than the amount of  $\text{H}_2$  contained in the formed  $\text{CH}_4$  (yellow line); moreover, in most catalysts,  $\text{H}_2$  loss is larger than the  $\text{H}_2$  required by  $\text{CO}_2$  methanation (green line). Hence, the remnant of  $\text{H}_2$  loss may be associated with the production of water or hydrogenated compounds not detected by GC, indicating that methanation would have a secondary role in the  $\text{H}_2$  loss during the syngas cleanup. On the other hand, CO conversion grows faster compared to the contribution of methanation (Figure 4b). Xu et al. [16] studied a Rh/ $\text{Al}_2\text{O}_3$  catalyst and proposed that at temperatures above  $150^\circ\text{C}$ , the methanation of  $\text{CO}_2$  formed during the CO-PROX facilitates the CO oxidation caused by changes in the  $\text{C-O}^*$  and  $\text{H}^*$  adsorbed species. This possible beneficial effect of CO-PROX and subsequent  $\text{CO}_2$  methanation seems to be stronger in some catalysts (e.g., AuCu/ $\text{CeO}_2\text{-Al}_2\text{O}_3$  and AuCu/ $\text{CeO}_2\text{-SiO}_2$ ), which would explain their higher activity at high temperatures (Figure 2d), where most  $\text{CH}_4$  was produced (Figure A2 in Appendix A). AuCu/ $\text{CeO}_2$  and AuCu/ $\text{La}_2\text{O}_3$  show an atypical trend (Figure 4b), where the CO conversion decreases with the  $\text{CH}_4$  formation, which could depend on the intermediates of  $\text{C-O}^*$  formed on these catalysts, as will be discussed later. Therefore, these results would confirm the beneficial effect of  $\text{CO}_2$  methanation during the CO-PROX proposed in [16], but it was also identified that this effect depends on the support and composition of the syngas.

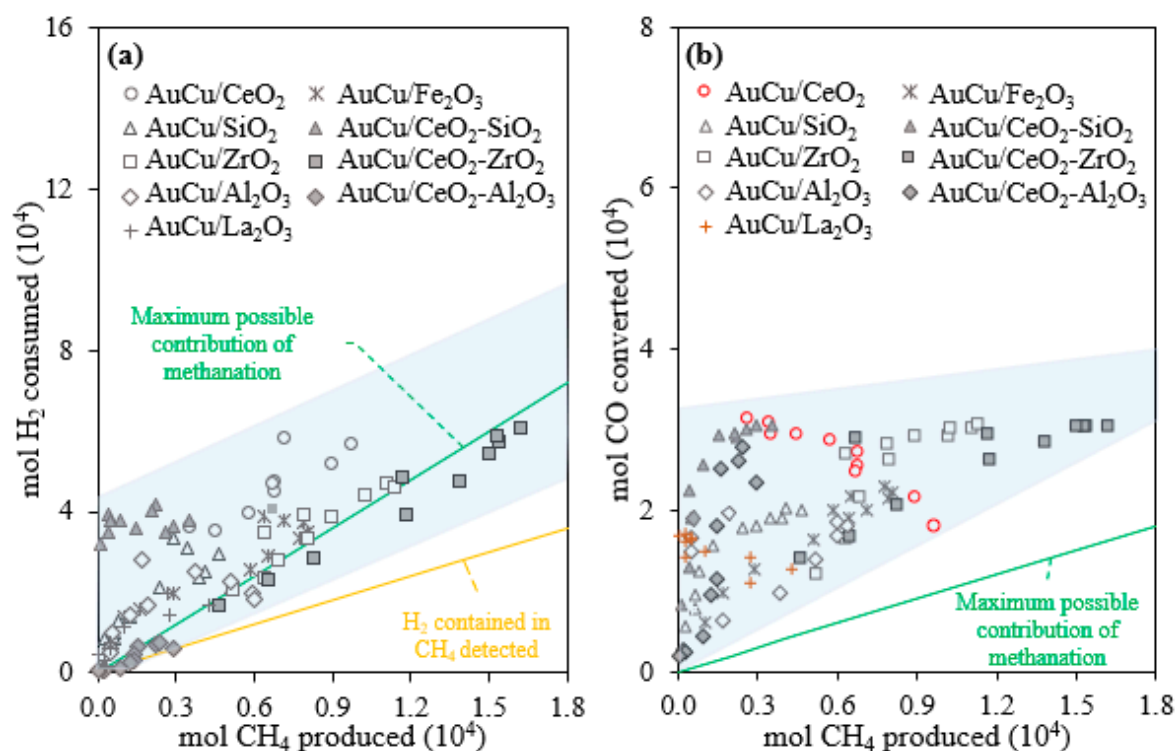


**Figure 4.** Contribution of methanation in (a) the  $\text{H}_2$  consumption and (b) CO conversion during the CO removal from an actual syngas. The shaded area conveys the trend of the experimental data.

Although the main objective in the cleaning of the syngas is the CO removal, differences in the activity and selectivity could lead to changes in product distribution over prolonged periods of operation. Therefore, the stability of Au–Cu catalysts loaded on the best single ( $\text{CeO}_2$ ) and dual support ( $\text{CeO}_2\text{-SiO}_2$ ) was evaluated. Figure 5 shows the product distribution over time obtained from a system consisting of ESR and cleanup reactors, the latter of which is packed with either

AuCu/CeO<sub>2</sub> or AuCu/CeO<sub>2</sub>-SiO<sub>2</sub>. In both cases, a H<sub>2</sub>-rich stream is obtained. However, AuCu/CeO<sub>2</sub> shows more variability in product distribution, and after around 42 h of operation deactivation was observed, at which point the test was stopped. In contrast, the AuCu/CeO<sub>2</sub>-SiO<sub>2</sub> catalyst ensures a stable operation for longer periods of time (at least 30% more time-on-stream, Figure 5b) with CO concentration of about 1000 ppm. The results of the stability test show that the use of dual metal oxides leads to less active (i.e., CO concentration of 1000 ppm versus 75 ppm) but more stable materials, which could be more interesting in extended processes.

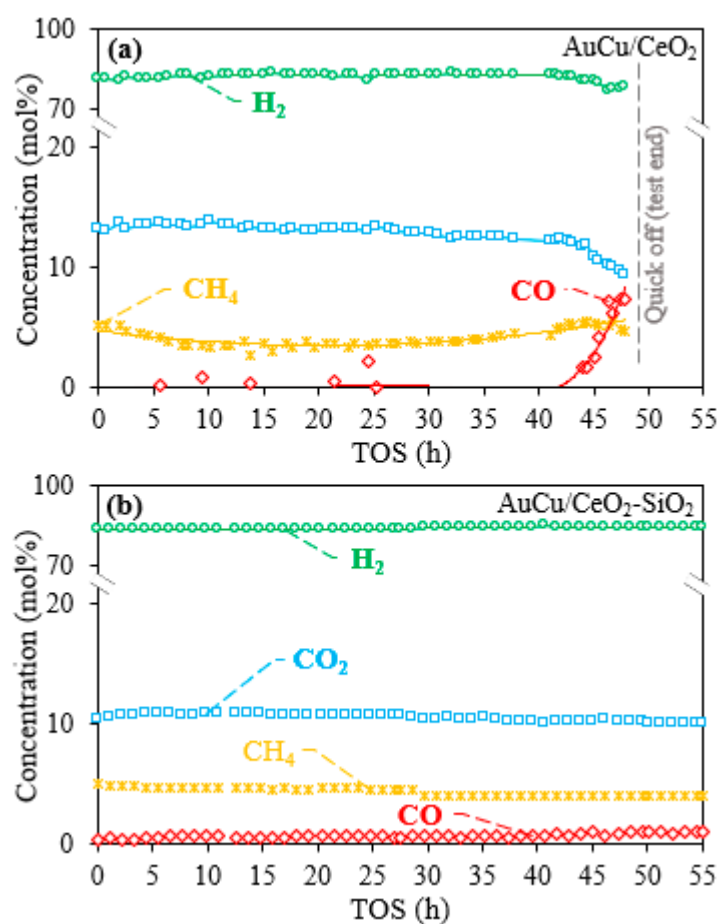


**Figure 5.** Products distribution obtained from a system that integrate the ESR reactor and the cleanup reactor, where the CO removal is performed with (a) AuCu/CeO<sub>2</sub> and (b) AuCu/CeO<sub>2</sub>-SiO<sub>2</sub> catalysts. Syngas feed: 7.8% H<sub>2</sub>, 2.0% CO, 0.5% CO<sub>2</sub>, 0.3% CH<sub>4</sub>, 1.4% H<sub>2</sub>O, 1.8% O<sub>2</sub>, 6.8% N<sub>2</sub>, and 79.4% Ar. Reaction conditions: The space velocity (SV) = 6.5 ± 0.2 L/g<sub>cat</sub>\*min and 0.3 g of the catalytic bed. Note: TOS = Time-on-stream.

Activity, H<sub>2</sub> consumption, and stability were used as criteria for comparison among the Au–Cu-supported catalysts for the CO removal from an actual syngas. Now, catalytic properties, such as reducibility, surface area, OSC, carbon deposit formation, and the CO-support interactions, will be related to the activity, selectivity, and stability of the Au–Cu catalysts supported in single and dual metal oxides.

## 2.2. Catalysts Characterization

### 2.2.1. TPR

The redox properties of catalysts have a significant effect on CO oxidation and metal-support interactions [17]. Figure 6 shows the H<sub>2</sub>-TPR profiles for the Au–Cu catalysts supported on single and

dual metal oxides. Deconvolution peaks are presented to identify possible individual contributions in each reduction zone, but they are not intended to be exact. Contrary to bare supports (Figure A3 in Appendix A), discrepancies are observed between supported Au–Cu catalysts. The specific reduction temperatures for Au and Cu are very diverse in the literature, possibly because the reduction of metals strongly depends on the interaction with other species [48]. In this study, a first zone (<130 °C) observed was attributed to the reduction of Au<sup>3+</sup> and Au<sup>+</sup> nanoparticles [41]. The second zone (130 to 430 °C) was associated with the reduction of Cu, where at least three species [49] can be identified: ( $\alpha$ ) easily reducible CuO nano particles, ( $\beta$ ) particles of CuO dispersed that interact moderately with the support, and ( $\gamma$ ) isolated particles of Cu [50]. In the last zone (>430 °C), the reduction of surface layers and bulk of the support is likely happening [34]. The  $\alpha$  and  $\beta$  species promote the formation of oxygen vacancies [51], contributing to the CO oxidation. Thus, preferential formation of CuO species in single and dual metal supports would explain the increase in CO<sub>2</sub> production over Au–Cu-supported catalysts compared to bare supports (Figures A1 and A2 in Appendix A).

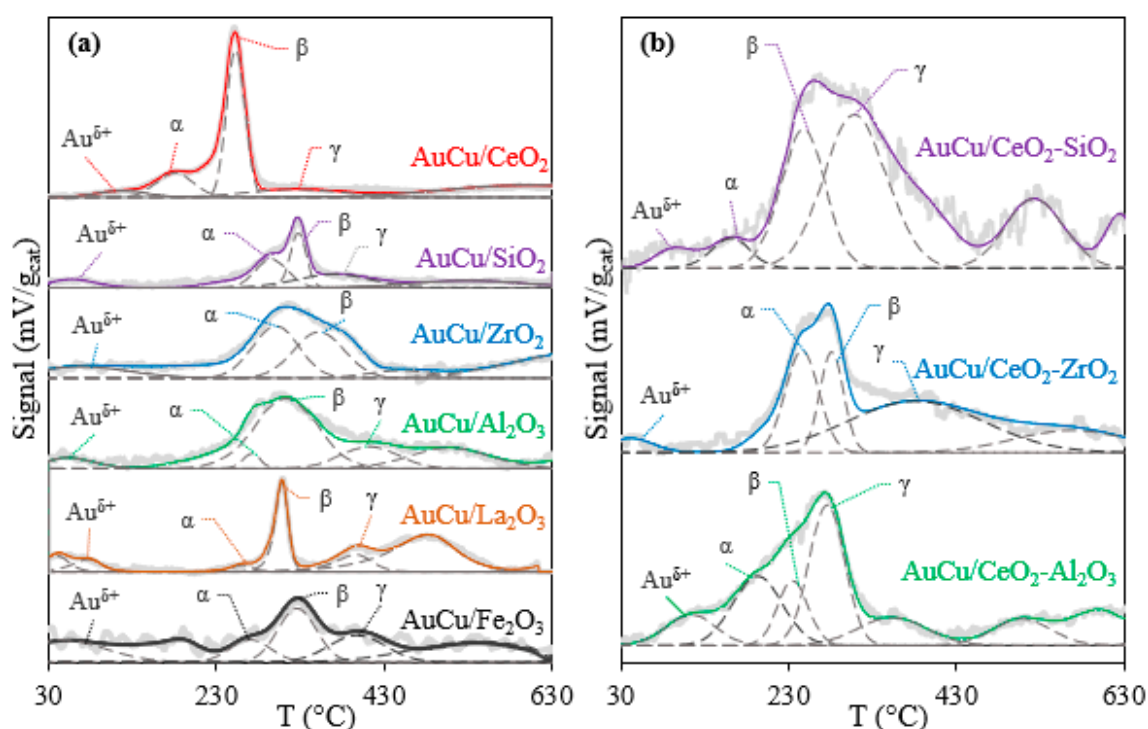


**Figure 6.** H<sub>2</sub>-temperature programmed reduction (TPR) profiles for Au–Cu catalysts supported on (a) single and (b) dual metal oxides.

On the other hand, the displacement of the reduction peaks to lower temperatures has been associated with changes in metal-support interactions [48]. CeO<sub>2</sub> shows an exceptional ability to facilitate the reduction of Cu and the formation of (mostly)  $\beta$  species. This effect has been previously studied [9,52], correlating a stronger CuO–CeO<sub>2</sub> interaction with high activity during CO-PROX. However, the increase in the contribution of  $\gamma$ -species and a slight shift of reduction peaks to higher temperatures could indicate a variation of the CuO–CeO<sub>2</sub> interaction in the Au–Cu catalysts supported in dual oxides. Thus, a change in the redox properties of the support caused by the presence of a second metal oxide could explain why the Au–Cu catalysts supported on dual oxides (i.e., AuCu/CeO<sub>2</sub>–SiO<sub>2</sub>, AuCu/CeO<sub>2</sub>–ZrO<sub>2</sub>, and AuCu/CeO<sub>2</sub>–Al<sub>2</sub>O<sub>3</sub>) showed less activity compared to AuCu/CeO<sub>2</sub> (Figure 2). However, an exceedingly strong CuO-support interaction could also mitigate the formation of selective Au–Cu alloys [31]. In fact, AuCu/ZrO<sub>2</sub> and AuCu/CeO<sub>2</sub>–ZrO<sub>2</sub> show a significant contribution of  $\alpha$  species, which could be related to the high H<sub>2</sub> loss observed in these catalysts (Figure 3c,d). On the contrary, the combination of inert metal oxides such as Al<sub>2</sub>O<sub>3</sub> with CeO<sub>2</sub> could facilitate the migration

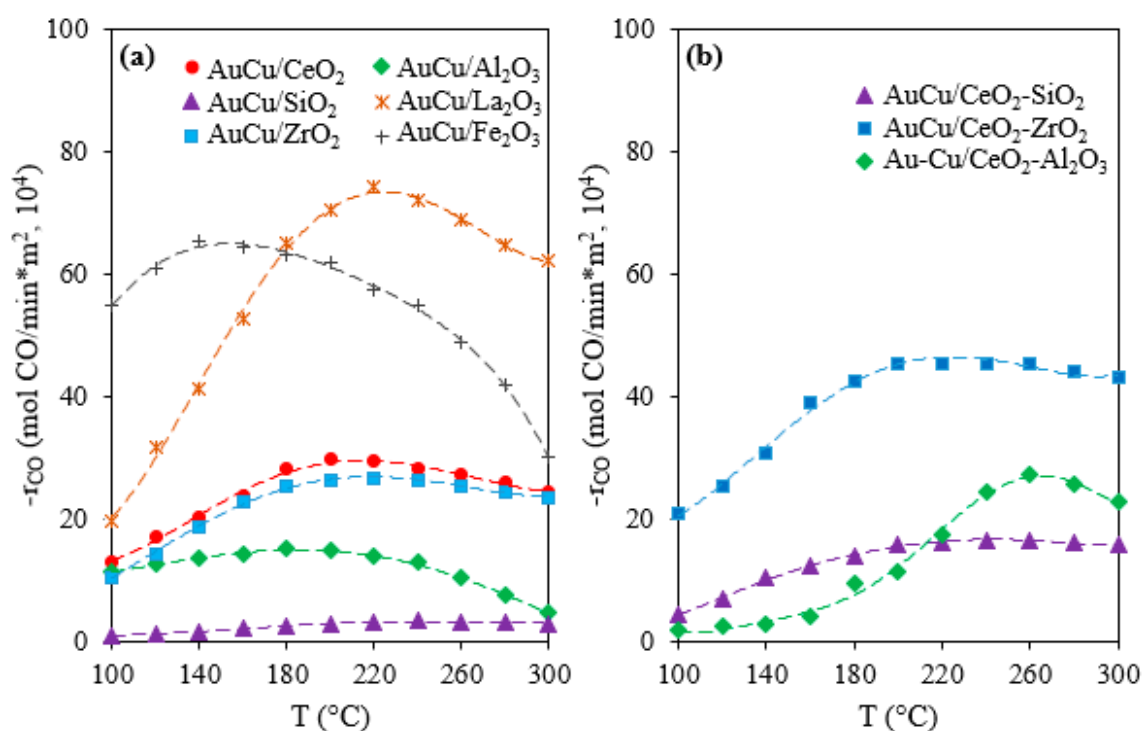
of CuO towards Au particles [31], leading to lower H<sub>2</sub> loss compared to single CeO<sub>2</sub> support. Then, the change in redox properties of CeO<sub>2</sub> by the presence of inert metal oxides (e.g., SiO<sub>2</sub>) could lead to less active but more selective materials during CO removal.

Table 1 shows the H/M index, which has been associated with apparent active metal dispersion [53]. The H/M index in AuCu/Fe<sub>2</sub>O<sub>3</sub> and AuCu/La<sub>2</sub>O<sub>3</sub> is particularly low, indicating that these catalysts are not as effective for dispersing active metals [53]. In the other catalysts, the H/M index was close to or larger than 1.0 (i.e., complete reduction of Au and Cu), which could be associated with a higher dispersion of Au and Cu on the catalytic surface. However, a high H/M value could also indicate an additional effect of superficial reduction of the supports by the interaction between metal oxides and active metals [54]. Au–Cu catalysts supported on dual metal oxides showed higher H/M index compared to their respective single supports, which could be associated with a favoring in the reduction of both active metals and support due to the interaction between metal oxides. If so, then the redox properties of Au–Cu catalysts supported on dual oxides would depend on several interactions: (i) active metal–active metal; (ii) active metal–support, and (iii) oxide I–oxide II. The variation of these interactions influences catalytic performance during CO removal.

### 2.2.2. BET Area

The surface area of the catalysts is key to the availability of the active sites and catalytic performance [55]. The BET area (Table 1) of the catalysts supported on basic oxides (i.e., CeO<sub>2</sub>, ZrO<sub>2</sub> and La<sub>2</sub>O<sub>3</sub> [56]) is larger than their respective bare supports (Table A1 in Appendix B), which has been previously associated with the formation of high disperse  $\beta$  species [20,57]. On the other hand, AuCu/Fe<sub>2</sub>O<sub>3</sub> and AuCu/La<sub>2</sub>O<sub>3</sub> show low surface areas, which match to the low capacity of these metal oxides to disperse active metals (low H/M index, Table 1). The synthesis method of the catalysts could influence the surface area of the support, overcoming some drawbacks of metal oxides such as Fe<sub>2</sub>O<sub>3</sub> by using alternative synthesis methods [32,58]. In contrast, the higher surface area of AuCu/CeO<sub>2</sub>-Al<sub>2</sub>O<sub>3</sub> and AuCu/CeO<sub>2</sub>-SiO<sub>2</sub> could favor the dispersion of Au and Cu, which is reflected by a larger H/M index (Table 1).

Although an increase in the surface area could contribute to improving the catalytic activity [55], the trend for surface area of the catalysts does not match their activity (Figure 2), indicating that the supports have other features that could be more relevant during the CO removal. Figure 7 shows the conversion rate of CO normalized by the surface area of catalysts. AuCu/La<sub>2</sub>O<sub>3</sub> has a high normalized activity, possibly because the basic supports promote the formation of Au nanoparticles [33] and formation of  $\beta$  species [20,57], which are active in the CO conversion. In fact, basic oxides, such as CeO<sub>2</sub> and ZrO<sub>2</sub>, also have higher normalized activity compared to less basic supports, such as Al<sub>2</sub>O<sub>3</sub> and SiO<sub>2</sub>. Also, the normalized activity of the AuCu/CeO<sub>2</sub>-ZrO<sub>2</sub> catalyst increases compared to their respective single supports. Recently, it was reported that the replacement of Zr<sup>4+</sup> ions in the lattice of the CaO-CeO<sub>2</sub> system leads to the formation of highly basic sites [59]. Then, we speculate that the high interaction in CeO<sub>2</sub>-ZrO<sub>2</sub> observed by TPR could lead to the formation of sites with greater basicity. However, the low surface area of basic supports is a well-known limitation that affects their activity [6]. So, because of the possible role of basic sites in CO removal, the design of catalysts for CO removal should include a support with both a high surface area and elevated basicity. Modifications in the morphology of metal oxides have been proposed as a successful strategy to achieve this objective in other catalytic processes [60]. Then, preparation of Au–Cu catalysts supported on single and dual metal oxides can be optimized to improve their catalytic properties during CO removal.



**Figure 7.** CO conversion rate normalized by the surface area of the Au–Cu catalysts supported in (a) single and (b) dual metal oxides.

### 2.2.3. OSC Measurements

The OSC of the support plays a central role in the oxidation of CO adsorbed on active sites [27]. Table 1 shows the OSC of Au–Cu catalysts supported on single and dual metal oxides. In general, the OSC of supported Au–Cu catalysts is higher than that of the bare supports (Table A1 in Appendix B), indicating that the presence of Au and Cu favors greater oxygen mobility in the catalyst. Also, the presence of  $\alpha$  and  $\beta$  species has been associated with the formation of oxygen vacancies on the catalytic surface [52]. Catalysts that have a higher OSC at 300 °C (i.e., AuCu/CeO<sub>2</sub>-ZrO<sub>2</sub>, AuCu/CeO<sub>2</sub>, AuCu/CeO<sub>2</sub>-SiO<sub>2</sub>, and AuCu/ZrO<sub>2</sub>) were the most active (Figure 2), but also those that showed the highest consumption of H<sub>2</sub> (Figure 3). However, the OSC depends strongly on the temperature: at 100 °C, all catalysts except AuCu/Al<sub>2</sub>O<sub>3</sub> showed an OSC up to 60% lower compared to 300 °C, which could be related to the lower activity of catalysts at low temperatures (Figure 2).

Likewise, the CO<sub>2</sub> formation depends on the availability of surface oxygen [15]. The first CO pulse (OSC) in AuCu/CeO<sub>2</sub> only corresponds to 39% of its oxygen storage complete capacity (OSCC), indicating that oxygen adsorbed on CeO<sub>2</sub> may not be easily released. The possible deficiency of CeO<sub>2</sub> to release the oxygen absorbed on its surface could limit the oxidation of carbon intermediates, which could, in turn, be related to the atypical trend observed in Figure 4b. The OSC in supports with larger surface area (i.e., AuCu/SiO<sub>2</sub>, AuCu/Al<sub>2</sub>O<sub>3</sub>, AuCu/CeO<sub>2</sub>-SiO<sub>2</sub>, and AuCu/CeO<sub>2</sub>-Al<sub>2</sub>O<sub>3</sub>), on the other hand, corresponds to more than 50% of their OSCC. A higher availability of surface oxygen (> OSC/OSCC) could be associated with the strong effect of CO<sub>2</sub> methanation on the CO removal for AuCu/CeO<sub>2</sub>-SiO<sub>2</sub> and AuCu/CeO<sub>2</sub>-Al<sub>2</sub>O<sub>3</sub>, as previously discussed. If so, then the beneficial effect of methanation during the CO-PROX proposed by [16] could be enhanced in catalysts that combine a high OSC and readiness to release their adsorbed oxygen (i.e., high OSC/OSCC ratio), which would require a high surface area.

On the other hand, the OSCC of the catalysts used decreases with respect to the fresh, activated ones (AC samples), reaching up to 73% reduction with AuCu/La<sub>2</sub>O<sub>3</sub>. This reduction could be associated with progressive oxidation of the catalyst surface by the presence of oxidants in the gas stream and deposits on the catalytic surface [20], conducive of a progressive deactivation. To clarify this, a TGA study was conducted.

#### 2.2.4. TGA

Table 3 shows the weight loss of Au–Cu catalysts supported on single and dual metal oxides. Most AC samples show a weight loss of less than 1% that could correspond to a remnant of the precursors of the active metals. However, AuCu/Fe<sub>2</sub>O<sub>3</sub> and AuCu/CeO<sub>2</sub>-SiO<sub>2</sub> show an increase in weight that can be associated with an oxygen adsorption; specifically, the CeO<sub>2</sub>-SiO<sub>2</sub> system can form a Ce<sub>9.33</sub>(SiO<sub>4</sub>)·6O<sub>2</sub> phase that is susceptible to consume oxygen above 600 °C [6]. The used catalysts have a higher weight loss than the fresh, activated ones (AC samples), indicating the presence of compounds deposited on the catalytic surface during the reaction. To determine the nature of the deposits, the TGA results were analyzed by weight loss in terms of rate of carbon equivalent formed in each temperature interval (Table 3). In the first interval (40–250 °C), light compounds, such as water, and adsorbed OH<sup>−</sup> and gases are released [28]; in this interval, AuCu/SiO<sub>2</sub> and AuCu/Al<sub>2</sub>O<sub>3</sub> showed the highest weight loss, which could be related to their high surface area, which favors moisture adsorption. In the second interval (250–600 °C), light hydrocarbons are oxidized [26]; AuCu/La<sub>2</sub>O<sub>3</sub> and AuCu/Fe<sub>2</sub>O<sub>3</sub> had the highest rate of carbon formation in this interval, which would explain the strong decrease in the OSCC and surface area, respectively, observed in these samples (Table 1). In the last interval (600–1000 °C), heavy hydrocarbons are oxidized, which are the type of deposits that could favor a faster deactivation of the catalyst [56]; in this zone, AuCu/CeO<sub>2</sub> showed a higher rate of carbon formation. Thus, rapid deactivation observed in AuCu/CeO<sub>2</sub> (Figure 5) could be associated with the decrease in surface area (17%, Table 1) and OSCC (59%, Table 1) promoted by the accumulation of deposits on the catalytic surface (Table 3). The formation of stable deposits could be associated with the formation of intermediates during the CO removal [28]; therefore, in situ DRIFTS was carried out to identify how the interaction between CO and support affects the performance of the supported Au–Cu catalysts.

**Table 3.** Weight loss of Au–Cu catalysts supported on single and dual supports evaluated in CO removal from an actual syngas.

Catalyst	Total Weight Loss (%)		Weight Loss of Spent Catalyst Samples by Temperature Intervals (mg of C/g <sub>cat</sub> *h)		
	AC	Spent	40–250 °C	250–600 °C	600–1000 °C
AuCu/CeO <sub>2</sub>	0.7	3.8 (U) 5.6 (S)	17.1 (U) 14.5 (S)	6.8 (U) 15.1 (U)	11.8 (U) 18.1 (U)
AuCu/SiO <sub>2</sub>	0.3	3.7 (U)	35.5 (U)	3.4 (U)	3.9 (U)
AuCu/ZrO <sub>2</sub>	0.9	1.6 (U)	9.2 (U)	2.1 (U)	4.7 (U)
AuCu/Al <sub>2</sub> O <sub>3</sub>	0.5	3.7 (U)	28.9 (U)	2.1 (U)	9.4 (U)
AuCu/La <sub>2</sub> O <sub>3</sub>	0.6	2.1 (U)	9.2 (U)	7.5 (U)	2.4 (U)
AuCu/Fe <sub>2</sub> O <sub>3</sub>	−0.3	2.5 (U)	18.4 (U)	8.9 (U)	NR
AuCu/CeO <sub>2</sub> -SiO <sub>2</sub>	−0.9	0.3 (U) 1.3 (S)	3.9 (U) 15.8 (S)	4.8 (U) 4.1 (U)	NR NR
AuCu/CeO <sub>2</sub> -ZrO <sub>2</sub>	0.5	1.7 (U)	9.2 (U)	6.2 (U)	0.8 (U)
AuCu/CeO <sub>2</sub> -Al <sub>2</sub> O <sub>3</sub>	0.6	2.6 (U)	17.1 (U)	2.7 (U)	7.1 (U)

Note: AC = activated catalyst, which were reduced with H<sub>2</sub> and stabilized in air before activity tests; U = sample used to obtain light-off curves; S = sample evaluated in the stability test; NR = Not reported.

### 2.2.5. In Situ DRIFTS

Figure 8 shows the DRIFTS spectra of CO adsorption on bare supports and supported Au–Cu catalysts.  $\text{CeO}_2$  and  $\text{ZrO}_2$  show higher intensity in the area associated with hydroxyl groups ( $\sim 3500\text{ cm}^{-1}$ ) that contributes to the CO conversion [36], which would explain their high activity among single metal oxides (Figure 2). Although the CO pulses were free of  $\text{H}_2$  or water, hydroxyl groups may be formed from the interaction of  $\text{H}_2$  with the surface of the support [61], which could occur during the  $\text{H}_2$  reduction that was performed on the AC samples. In fact, Zhou et al. [62] studied the CO adsorption on bare  $\text{ZrO}_2$  by DRIFTS and Fourier Transform Infrared Spectroscopy (FTIR), identifying up to three families of hydroxyl groups in the zone from  $3675$  to  $3772\text{ cm}^{-1}$ , which are activated by the adsorption of CO, even at room temperature, and have an active role in the formation of surface intermediates.  $\text{CeO}_2$  favors the formation of hydroxyl groups even with the first pulse of CO, which could be decisive in ensuring a syngas with a lower CO concentration. In the C–O\* zone ( $1200$  to  $1700\text{ cm}^{-1}$  [63]), the formation of bidentate carbonates ( $1600\text{ cm}^{-1}$ ) and formates ( $1300$  and  $1500\text{ cm}^{-1}$ ) are observed, which are also intermediates in the CO conversion [20,51,63]. The formation of hydroxyl groups and C–O\* species were lower than dual supports when compared to  $\text{CeO}_2$ ; specifically,  $\text{CeO}_2\text{-Al}_2\text{O}_3$  shows a significant reduction in the formation of C–O\* intermediates, which would correspond to its lower activity among the dual supports (Figure 2).

The inclusion of Au–Cu in the single oxides (Figure 8c) favors the presence of hydroxyls and the formation of C–O\* intermediates, possibly due to the ability of Au to form Au–CO and Au–OOH species [36]. In fact, most catalysts show an increase in CO adsorbed ( $2100\text{ cm}^{-1}$ ), which is associated with CO–Au<sup>0</sup> species [64], indicating that Au could be present mostly as Au<sup>0</sup> on the catalytic surface, as previously reported for systems such as Au/ $\text{CeO}_2$  [20] and Au/ $\text{La}_2\text{O}_3/\text{Al}_2\text{O}_3$  [33], evaluated by XPS. However, in AuCu/ $\text{CeO}_2\text{-SiO}_2$  and AuCu/ $\text{CeO}_2\text{-ZrO}_2$ , a weak peak of CO adsorption between  $2075$  and  $2050\text{ cm}^{-1}$  is also observed, which has been associated with the formation of CO–Au <sup>$\delta^-$</sup>  species [65]. In the case of AuCu/ $\text{CeO}_2\text{-ZrO}_2$ , the formation of these species only occurs after several CO pulses. The presence of Au <sup>$\delta^-$</sup>  has been related to a stronger support-metal interaction, which could be ascribed to the high stability of AuCu/ $\text{CeO}_2\text{-SiO}_2$  (Figure 5).

The formation of C–O\* intermediates may occur on different active sites, including Au<sup>0</sup>, Au <sup>$\delta^-$</sup> , and CuO, but the formation of carbonate species at approximately  $1470\text{ cm}^{-1}$  occurs preferably on Cu<sup>+</sup> species [66], which are very active in CO-PROX [67]. The peak associated with Cu<sup>+</sup> is well defined in AuCu/ $\text{CeO}_2$ . Furthermore, the formation of active Cu<sup>+</sup> species due to the high affinity in CuO– $\text{CeO}_2$  has been extensively studied by XPS and DRIFTS [25,68]. Thus, a smaller amount of Cu<sup>+</sup> species on the other catalysts could explain their inability to ensure CO concentrations below 100 ppm (Table 1). Besides, the peaks associated with formate species, which are related to  $\text{CH}_4$  formation, are better defined on  $\text{CeO}_2$ . It is accepted that  $\text{CH}_4$  formation is promoted on several oxides (e.g.,  $\text{Al}_2\text{O}_3$ ,  $\text{ZrO}_2$ ,  $\text{Y}_2\text{O}_3$ , MgO, and  $\text{CeO}_2$  [69]), but the special ability to adsorb and activate carbon species makes  $\text{CeO}_2$  an adequate support in  $\text{CO}_2$  methanation and CO-SMET [70]. Nevertheless, during the CO removal the Boudouard reaction and the  $\text{CH}_4$  decomposition could contribute to the production of carbon deposits [26], favoring the catalyst deactivation. Then, the ability of  $\text{CeO}_2$  to form C–O\* intermediates (Figure 8) assisted by Cu<sup>+</sup> species and its lower capacity to release the surface oxygen (low OSC/OSCC) could contribute to the generation of stable carbon deposits, as was observed by TGA, leading to its rapid deactivation (Figure 5). Besides, the deficiency of AuCu/ $\text{CeO}_2$  to mitigate carbon deposition due to the excessive formation of C–O\* intermediates could be also related to the atypical behavior of  $\text{CH}_4$  formation (Figure 4b). However, the less active materials show low formation of intermediates (e.g., AuCu/ $\text{La}_2\text{O}_3$ , AuCu/ $\text{Fe}_2\text{O}_3$ , and AuCu/ $\text{SiO}_2$ ). Thus, the selection of the support for the CO removal from a syngas must consider the balance between activity and stability.

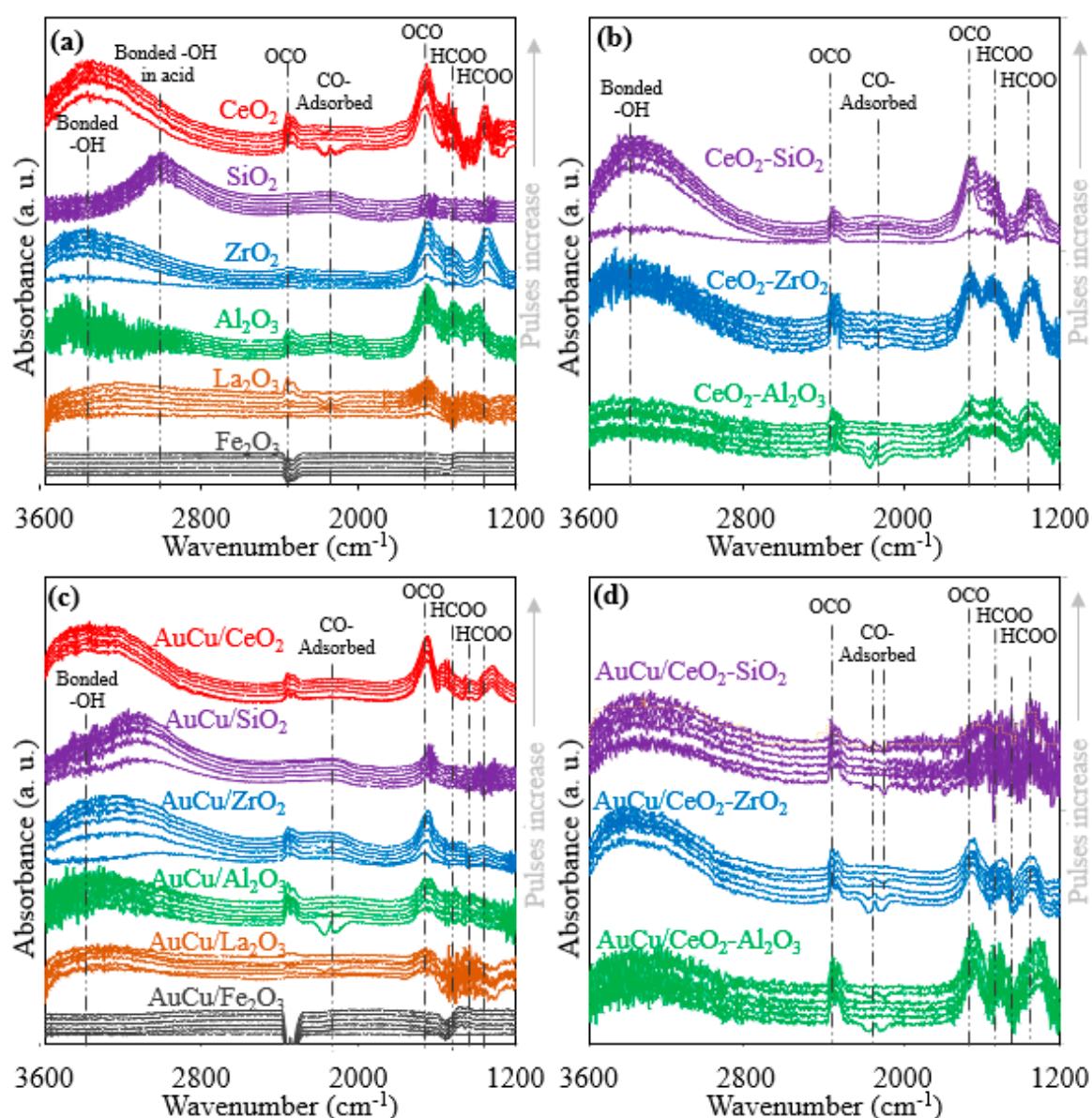


**Figure 8.** In situ diffuse reflectance infrared Fourier transform spectroscopy (DRIFTS) of CO adsorption of (a,b) bare supports and (c,d) supported Au–Cu catalysts.

The results of DRIFTS support the notion that the use of dual metal oxides favors less active but more stable catalysts. Therefore, in this study,  $\text{CeO}_2$  is presented as the most promising support for developing a compact system to carry out the CO removal from an actual syngas. However, the selectivity and stability of  $\text{CeO}_2$  require improvements. Furthermore, it was shown that the use of dual supports, specifically  $\text{CeO}_2\text{-SiO}_2$  and  $\text{CeO}_2\text{-ZrO}_2$ , could be a promising strategy to overcome the deficiencies presented by  $\text{CeO}_2$ .

### 3. Materials and Methods

#### 3.1. Support Selection

The supports evaluated in this work were selected according to a literature review, and are summarized in Figure 1. Scientific articles published between 2012 and 2019 that included at least one of the following reactions were reviewed: CO-PROX, WGS, and CO-SMET. The detailed list of reviewed articles can be consulted in Table A2 (see Appendix B).

### 3.2. Catalyst Synthesis

The single supports of CeO<sub>2</sub>, ZrO<sub>2</sub>, and Fe<sub>2</sub>O<sub>3</sub> were obtained by calcination at 500 °C for 2 h of Ce(NO<sub>3</sub>)<sub>3</sub>·6H<sub>2</sub>O (CAS: 10294-41-4, Sigma Aldrich, Saint Louis, MO, USA), ZrO(NO<sub>3</sub>)<sub>2</sub>·xH<sub>2</sub>O (CAS: 14985-18-3, Sigma Aldrich, Saint Louis, MO, USA), and Fe(NO<sub>3</sub>)<sub>3</sub>·9H<sub>2</sub>O (CAS: 7782-61-8, Merck, Darmstadt, HE, Germany), respectively. Also, commercial oxides of La<sub>2</sub>O<sub>3</sub> (CAS: 1312-81-8, Sigma Aldrich, Saint Louis, MO, USA), Al<sub>2</sub>O<sub>3</sub> (CAS: 1344-28-1, Sigma Aldrich, Saint Louis, MO, USA), and SiO<sub>2</sub> (CAS: 60676-86-0, Merck, Darmstadt, HE, Germany) were used, which were also calcined at 500 °C in a muffle for 2 h.

Dual supports of CeO<sub>2</sub>-ZrO<sub>2</sub>, CeO<sub>2</sub>-Al<sub>2</sub>O<sub>3</sub>, and CeO<sub>2</sub>-SiO<sub>2</sub> were obtained from aqueous solutions of Ce(NO<sub>3</sub>)<sub>3</sub>·6H<sub>2</sub>O (CAS: 10294-41-4, Sigma Aldrich, Saint Louis, MO, USA) with ZrO(NO<sub>3</sub>)<sub>2</sub>·H<sub>2</sub>O (CAS: 14985-18-3, Sigma Aldrich, Saint Louis, MO, USA), Al<sub>2</sub>O<sub>3</sub> (CAS: 1344-28-1, Sigma Aldrich, Saint Louis, MO, USA), and SiO<sub>2</sub> (CAS: 60676-86-0, Merck, Darmstadt, HE, Germany), respectively, ensuring a molar ratio of Ce/M = 1 (M = Si, Zr and Al). Each solution was dried at 80 °C for 24 h and calcined at 500 °C in a muffle for 4 h. All supports (i.e., single and dual metal oxides) were screened with a 140-mesh sieve.

Bimetallic Au–Cu catalysts supported on each single and dual metal oxide were prepared according to the procedure described in [20], ensuring active metal loads of Au (1 wt%) and Cu (1 wt%). Au was first impregnated on each support by the precipitation-deposition method at pH 6 and 80 °C, using a solution of HAuCl<sub>4</sub>·3H<sub>2</sub>O (CAS: 16961-25-4 Sigma Aldrich, MO, USA). The filtered solid was dried at 80 °C for 24 h. Subsequently, Cu was included in the Au catalysts by the incipient wetness impregnation method, using a solution of Cu(NO<sub>3</sub>)<sub>2</sub>·3H<sub>2</sub>O (CAS: 10031-43-3, Sigma Aldrich, Saint Louis, MO, USA). The catalyst obtained was dried at 80 °C for 24 h, calcined at 500 °C in a muffle for 2 h, and screened with a 140-mesh sieve.

The RhPt/CeO<sub>2</sub>-SiO<sub>2</sub> catalyst for ESR was prepared according to the methodology described in [6]. Briefly, CeO<sub>2</sub>-SiO<sub>2</sub> support was obtained from Ce(NO<sub>3</sub>)<sub>3</sub>·6H<sub>2</sub>O (CAS: 10294-41-4, Sigma Aldrich, Saint Louis, MO, USA) and SiO<sub>2</sub> (CAS: 60676-86-0, Merck, Darmstadt, HE, Germany) solutions, ensuring a molar ratio of Ce/Si = 2. Rh and Pt were deposited on the CeO<sub>2</sub>-SiO<sub>2</sub> support by the incipient wetness co-impregnation method, using RhCl<sub>3</sub>·H<sub>2</sub>O (CAS: 20765-98-4, Sigma Aldrich, Saint Louis, MO, USA) and H<sub>2</sub>PtCl<sub>6</sub>·6H<sub>2</sub>O (CAS: 10025-65-7, Sigma Aldrich, Saint Louis, MO, USA) solutions. The catalyst obtained was dried at 80 °C for 24 h, calcined at 700 °C for 2 h, and screened with a 140-mesh sieve.

### 3.3. Obtaining Syngas

The syngas was obtained from ESR with a RhPt/CeO<sub>2</sub>-SiO<sub>2</sub> catalyst at 700 °C in the first reactor (ESR reactor). The plug flow conditions in the ESR reactor were maintained ensuring  $L/Dp > 50$  ratios (i.e., catalytic bed height ( $L$ ) and catalyst particle size ( $Dp$ )) and  $D/Dp > 60$  (i.e., diameter internal to the reactor ( $D$ )), as recommended in [71]. The catalyst bed consisted of 0.050 g of RhPt/CeO<sub>2</sub>-SiO<sub>2</sub> and 0.250 g of inert quartz. The reactor feed consisted of 0.3 L/min of a mixture of ethanol (1.8 mol%), water (5.4 mol%), and Ar as carrier gas. The space velocity (SV) was set at  $6.4 \pm 0.2$  L/g<sub>cat</sub>\*min. The syngas obtained in the ESR reactor, containing H<sub>2</sub> (8.4 mol%), CO (2.2 mol%), H<sub>2</sub>O (1.6 mol%), CO<sub>2</sub> (0.6 mol%), CH<sub>4</sub> (0.3 mol%), and Ar (86.9 mol%), remained stable, with a variation <6.8%.

### 3.4. Catalytic Test

The supports and Au–Cu catalysts for the CO removal from the syngas were evaluated in a second reactor (cleanup reactor) between 100 and 300 °C. For this, the ESR reactor outlet was mixed with dry air, ensuring an excess oxygen factor ( $\lambda$ ) of  $1.8 \pm 0.05$  [20], and connected to the cleanup reactor inlet. The plug flow conditions in the cleanup reactor were maintained as previously described for the ESR reactor. The catalyst bed consisted of 0.050 g of catalyst (i.e., supports or Au–Cu catalysts) and 0.250 g of inert quartz. The SV in the cleanup reactor was set at  $6.5 \pm 0.3$  L/g<sub>cat</sub>\*min. Before the reaction, the supports and Au–Cu catalysts were pretreated in situ at 300 °C with streams of 8% H<sub>2</sub>/Ar for 1 h,

followed by Ar for 0.5 h, and finally 10% air/Ar for 0.5 h. These samples were labeled as “activated catalyst” (AC). Also, the samples used to obtain the light-off curves were labeled “U”, while those used in the stability test were labeled “S”.

The species at the outlet of each reactor (i.e., ESR reactor and cleanup reactor) were quantified by gas chromatography (GC) in a Clarus 580 (Perkin Elmer, Waltham, MA, USA), equipped with a Carboxen 1010 plot column (30 m, 0.53 mm ID, Restek, Bellefonte, PA, USA) connected to a thermal conductivity detector (TCD). Ar was used as carrier gas and N<sub>2</sub> as internal reference. The reaction conditions and GC data processed in Excel can be consulted in detail and downloaded from [72].

The conversion of CO ( $x_{CO}$ ), the production of the main products ( $Y_{CO_2}$  and  $Y_{CH_4}$ ), and the H<sub>2</sub> obtained ( $Y_{H_2}$ ) from the integrated system were obtained considering the molar flows ( $F_i$ ) to the output of each reactor (i.e., ESR reactor and cleanup reactor), according to Equations (1) and (3). Production of CO, CH<sub>4</sub>, and H<sub>2</sub> were normalized with the amount of carbon entering the system ( $F_{C, \text{inlet to the system}}$ ), which remained constant at  $5.2 \times 10^{-4}$  mol/min of C.

$$x_{CO} = \frac{F_{CO, \text{ ESR-reactor}} - F_{CO, \text{ cleanup-reactor}}}{F_{CO, \text{ ESR-reactor}}} \quad (1)$$

$$Y_{CH_4;CO_2} = \frac{F_{CH_4;CO_2, \text{ cleanup-reactor}} - F_{CH_4;CO_2, \text{ ESR-reactor}}}{F_{C, \text{ inlet to the system}}} \quad (2)$$

$$Y_{H_2} = \frac{F_{H_2, \text{ cleanup-reactor}}}{F_{C, \text{ inlet to the system}}} \quad (3)$$

### 3.5. Characterization Tests

The reducibility of supports and Au–Cu catalysts was determined by TPR. The experiments were carried out in a ChemBET Pulsar unit (Quantachrome Instruments, Boynton Beach, FL, USA) equipped with a TCD. Prior to the reduction,  $0.07 \pm 0.01$  g of AC samples was pretreated with N<sub>2</sub> (0.02 L/min) at 120 °C for 1 h and then cooled to room temperature. Subsequently, 5 % H<sub>2</sub>/N<sub>2</sub> was passed, and the temperature was increased to 700 °C (5 °C/min). The H<sub>2</sub> uptake was calculated by integrating the peaks associated with the reduction of active metals (i.e., Au and Cu). The apparent active metal dispersion (H/M ratio) was also determined [53], assuming that the adsorption stoichiometry is one hydrogen atom for one active metal atom (Au + Cu).

The surface area of the samples was determined by standard physisorption of N<sub>2</sub> in a ChemBET Pulsar unit (Quantachrome Instruments, Boynton Beach, FL, USA). For this,  $0.06 \pm 0.01$  g of sample was pretreated with N<sub>2</sub> (0.02 L/min) at 100 °C for 1 h and then cooled to room temperature for 0.5 h. Subsequently, the sample was immersed in a liquid N<sub>2</sub> bath. The BET area was measured with a single point, using 30% N<sub>2</sub>/He (0.02 L/min). The measurements were repeated until deviations lower than 5% were obtained.

The OSC values of the samples were measured in a ChemBET Pulsar unit (Quantachrome Instruments, Boynton Beach, FL, USA), according to the procedure described in [41]. Briefly,  $0.06 \pm 0.01$  g of sample was degassed in Ar (0.02 L/min) at 300 °C for 1 h. OSC was measured at 300 and 100 °C with independent samples. For this, 10 pulses of pure O<sub>2</sub> (0.25 mL) were injected to oxidize the sample, followed by a 20 min purge with Ar. Then, pulses of a 5 % CO/Ar mixture (0.25 mL) were injected until a constant signal was obtained. The OSC value was calculated by the CO consumed in the first pulse, and the OSCC value was determined by the total CO consumed.

The weight loss, associated with the presence of impurities, moisture, and carbon deposition in samples, was measured by TGA. The change in mass was determined using a thermogravimetric analyzer (Mettler Toledo, Columbus, OH, USA). For this,  $0.02 \pm 0.01$  g of sample was pretreated with a  $N_2$  (0.1 L/min) at 100 °C for 1 h and then cooled to 40 °C for 0.5 h. Subsequently, the sample was heated to 1000 °C (5 °C/min) in a dry air stream (0.1 L/min). Then, the rate of carbon formation was calculated according to Equation (4).

$$\text{Rate of carbon formation} = \frac{\text{Weight loss in term of C (mg)}}{\text{mass of catalyst (g)} * \text{TGA test time (h)}} \quad (4)$$

The CO adsorption on supports and catalysts was studied by in situ DRIFTS in a Nicolet iS10 spectrum device (Thermo Scientific, Waltham, MA, USA) equipped with a diffuse reflection attachment DRK-3 Praying Mantis (Harrick Scientific Products, New York, NY, USA). Spectra were taken between 400 and 4000  $cm^{-1}$ , with 64 scans per minute and a resolution of 4  $cm^{-1}$ . The sample holder was sealed with an airtight hood with ZeSn windows. In addition, the airtight hood was isolated with an Ar stream to avoid interference from the environment. Approximately 0.02 g of AC samples were degassed in Ar (15 mL/min) at 50 °C for 30 min. Then, 10 pulses of 30  $\mu$ L of CO, obtained from a certified 5% CO/Ar mixture, were injected into the cell; between each pulse, Ar (15 mL/min) was passed for 10 min.

Raw and processed Excel data for characterization tests can be downloaded from [72].

#### 4. Conclusions

Several single and dual metal oxides were investigated as supports in a catalytic system based on Au–Cu for the CO removal from an actual syngas. The use of a syngas obtained directly from the ESR affects the effectiveness in the CO removal; specifically, a low  $H_2/CO$  ratio could favor greater  $H_2$  loss. AuCu/CeO<sub>2</sub> was identified as the most active catalyst in the CO removal, but it also contributes to a higher  $H_2$  consumption.  $H_2$  is lost mainly by the formation of water and  $CH_4$ , where the occurrence of  $CO_2$  methanation affected the CO removal differently. Over CeO<sub>2</sub>-Al<sub>2</sub>O<sub>3</sub> and CeO<sub>2</sub>-SiO<sub>2</sub>, methanation seems to improve CO removal because the CO-PROX product,  $CO_2$ , is constantly consumed to produce  $CH_4$ . On the contrary, methanation has a negative effect on CeO<sub>2</sub> and La<sub>2</sub>O<sub>3</sub> because the formed  $CH_4$  favors carbon deposition.

Differences among the catalysts were evaluated by several characterization techniques. DRIFTS spectra of CO adsorption showed that CeO<sub>2</sub> has a superior activity because it favors the formation of C–O\* and OH<sup>−</sup> intermediates, but it promotes the formation of carbon deposits that lead to its deactivation. Similarly, TPR showed that ZrO<sub>2</sub> has a high interaction with active metals (Au–Cu), which makes it active but less selective, favoring a high  $H_2$  oxidation. In addition, the low OSC of Al<sub>2</sub>O<sub>3</sub> and SiO<sub>2</sub>, and the lower surface area of Fe<sub>2</sub>O<sub>3</sub> and La<sub>2</sub>O<sub>3</sub> make these metal oxides less active. Regarding dual supports, the inclusion of a second metal oxide weakens the interaction of CeO<sub>2</sub> with the active metals, reducing activity. However, dual metal oxides are more selective and stable than single CeO<sub>2</sub> because they mitigate the excess of C–O\* species, as was observed by DRIFTS; specifically, CeO<sub>2</sub>-SiO<sub>2</sub> mitigates the formation of stable carbon deposits that deactivate the catalyst. Thus, AuCu/CeO<sub>2</sub> was identified as a promising catalyst for carrying out the CO removal from a syngas using just one catalytic reactor, but improvements in CeO<sub>2</sub> stability are still required. Therefore, the use of dual supports (e.g., CeO<sub>2</sub>-SiO<sub>2</sub>) could be a strategy to overcome single CeO<sub>2</sub> deficiencies. Thus, the development of more compact systems for the purification of  $H_2$  suitable for FC implicitly promotes greater  $H_2$  consumption. The results of this work aim to contribute to the development and establishment of sustainable energies based on  $H_2$ .

**Author Contributions:** All the authors contributed to the development, writing, and review of this work.

**Funding:** This research was funded by Colciencias (Francisco Jose de Caldas Fund) and Universidad de La Sabana through the projects with code ING-163, ING-166, and ING-221 (Colciencias contracts 0608-2013, 174-2016 and 548-2019).

**Acknowledgments:** B. Cifuentes acknowledges Colciencias for the doctoral scholarship (grant number 727-2015). F. Bustamante acknowledges the support of the Environmental Catalysis Research Group of Universidad de Antioquia.

**Conflicts of Interest:** There are no conflicts of interest to declare.

## Appendix A

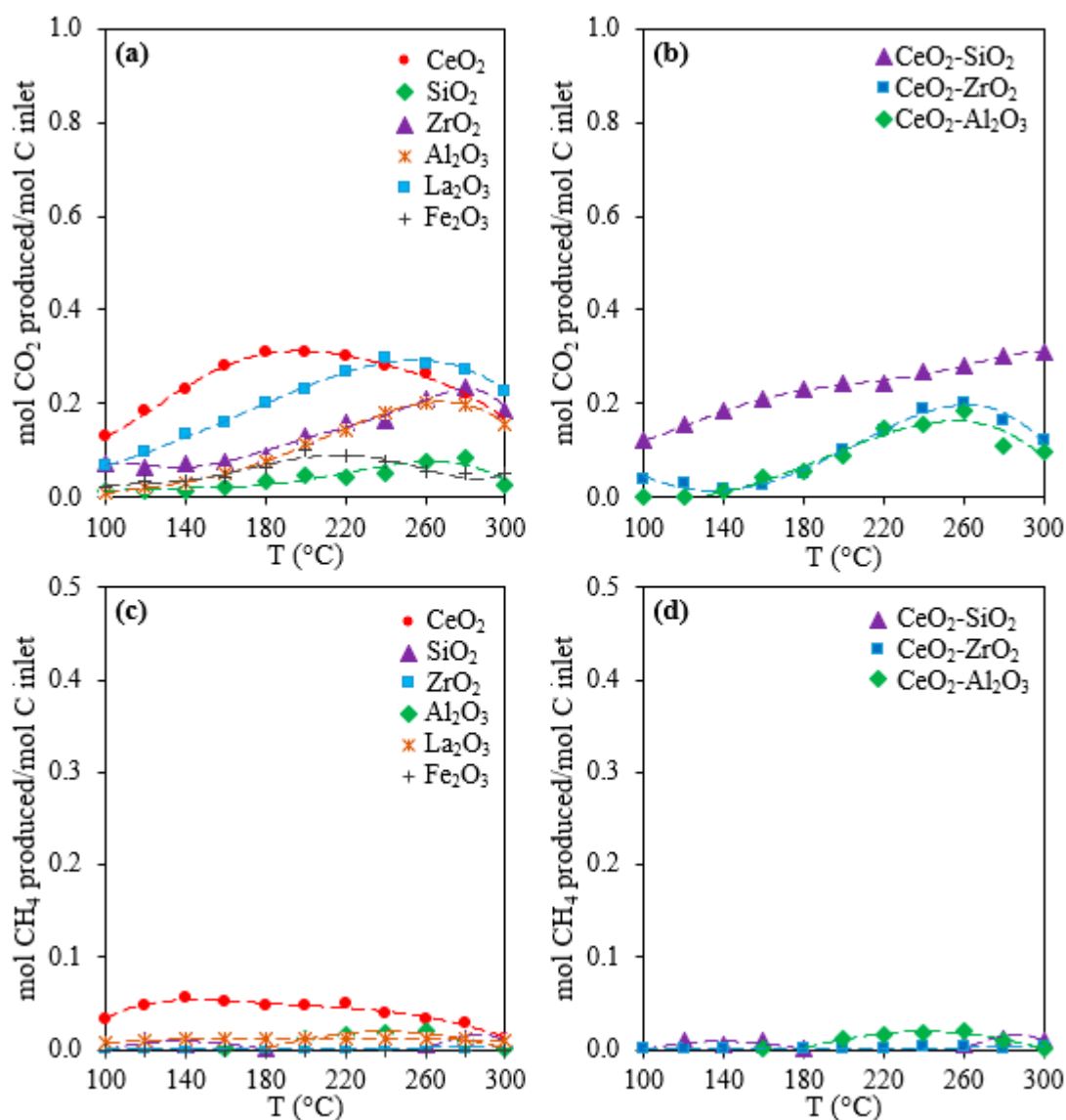


**Figure A1.** (a,b) CO<sub>2</sub> and CH<sub>4</sub> (c,d) production in the CO cleanup reactor with simple and dual supports. Syngas composition: 8.4% H<sub>2</sub>, 2.2% CO, 0.6% CO<sub>2</sub>, 0.3% CH<sub>4</sub>, 1.6% H<sub>2</sub>O, and Ar.  $\lambda = 1.8$ . Reaction conditions: SV = 6.5 ± 0.2 L/g<sub>cat</sub>\*min; 0.050 g of catalyst and 0.250 g of inert quartz.

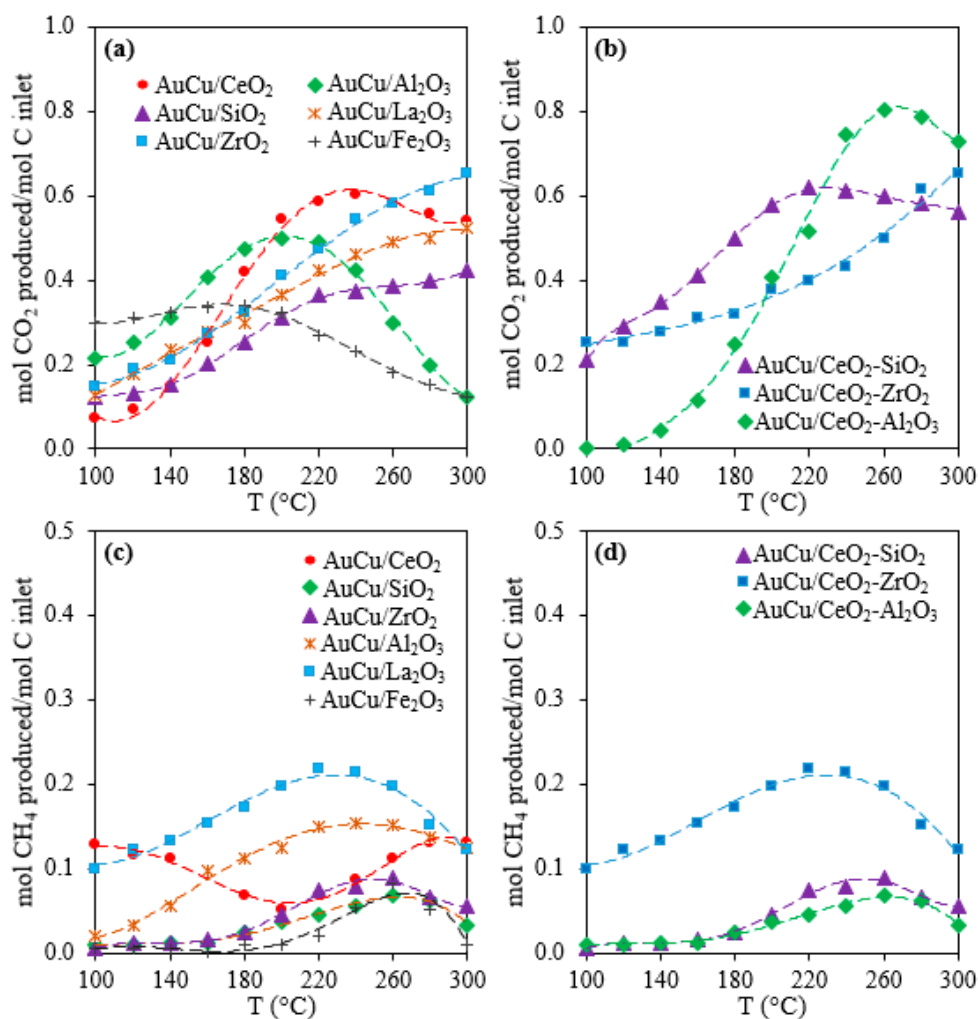


**Figure A2.** (a,b) CO<sub>2</sub> and CH<sub>4</sub> (c,d) production in the CO cleanup reactor with Au–Cu catalysts supported on simple and dual supports. Syngas composition: 8.4% H<sub>2</sub>, 2.2% CO, 0.6% CO<sub>2</sub>, 0.3% CH<sub>4</sub>, 1.6% H<sub>2</sub>O, and Ar.  $\lambda=1.8$ . Reaction conditions: SV =  $6.5 \pm 0.2$  L/g<sub>cat</sub>\*min; 0.050 g of catalyst and 0.250 g of inert quartz.

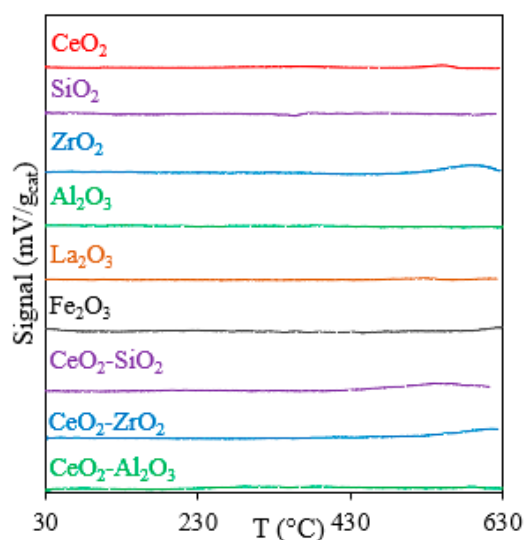


**Figure A3.** H<sub>2</sub>-TPR profiles of bare supports evaluated in the CO removal from an actual syngas.

## Appendix B

**Table A1.** Surface area, OSC, OSCC, and thermogravimetric analysis (TGA) results of single and dual supports.

Support	BET Surface Area (m <sup>2</sup> /gcat)		OSC in Fresh Samples at 300 °C (μmol O <sub>2</sub> /gcat)	OSCC in Fresh Samples at 300 °C (μmol O <sub>2</sub> /gcat)	Weight Loss (%)	
	Fresh	Used			Fresh	Used
CeO <sub>2</sub>	52.4	55.4	61	135	1.1	0.6
SiO <sub>2</sub>	466.5	410.6	41	49	1.4	1.1
ZrO <sub>2</sub>	51.6	44.9	55	99	1.6	0.6
Al <sub>2</sub> O <sub>3</sub>	96	68.6	36	55	1.7	0.2
La <sub>2</sub> O <sub>3</sub>	14.1	15.3	21	68	5.5	2.1
Fe <sub>2</sub> O <sub>3</sub>	38.1	36.7	5	16	0.7	0.8
CeO <sub>2</sub> -SiO <sub>2</sub>	163.2	155.2	54	105	-2.7	1.8
CeO <sub>2</sub> -ZrO <sub>2</sub>	44.3	40.5	46	110	0.2	2.0
CeO <sub>2</sub> -Al <sub>2</sub> O <sub>3</sub>	72.7	69.1	41	120	2.0	1.0

**Table A2.** Reviewed articles for the selection of supports evaluated in the CO removal.

Date	Active Metals	Metal Oxide I	Metal Oxide II	Journal	Digital Object Identifier (DOI)
2012	CuO	Fe <sub>2</sub> O <sub>3</sub>	-	Chemical Engineering Journal	10.1016/j.cej.2012.01.017
2012	Pt	Other	-	Electrochimica Acta	10.1016/j.electacta.2012.04.150
2012	-	Fe <sub>2</sub> O <sub>3</sub>	-	Applied Surface Science	10.1016/j.apsusc.2011.10.092
2012	-	NiO <sub>2</sub>	-	Journal of Molecular Catalysis A: Chemical	10.1016/j.molcata.2012.05.001
2013	Ni, Co	Co <sub>3</sub> O <sub>4</sub>	-	Journal of Alloys and Compounds	10.1016/j.jallcom.2013.04.053
2013	CuO	TiO <sub>2</sub>	Al <sub>2</sub> O <sub>3</sub>	Surface and Coatings Technology	10.1016/j.surfcoat.2012.10.031
2013	Co	Fe <sub>2</sub> O <sub>3</sub>	-	Chemical Engineering Journal	10.1016/j.cej.2013.02.002
2014	Co	MgO	-	Process Safety and Environmental Protection	10.1016/j.psep.2013.12.003
2014	Pt	CeO <sub>2</sub>	-	Chemical Engineering Journal	10.1016/j.cej.2014.06.058
2014	Pd	Fe <sub>2</sub> O <sub>3</sub>	-	Journal of Catalysis	10.1016/j.jcat.2014.06.019
2014	Ag	Zeolite	-	Fuel	10.1016/j.fuel.2014.07.011
2014	Au	NiO <sub>2</sub>	-	Applied Catalysis A: General	10.1016/j.apcata.2014.02.003
2014	CuO	SiO <sub>2</sub>	CeO <sub>2</sub>	Journal of Environmental Chemical Engineering	10.1016/j.jece.2014.03.021
2015	Co, Fe, Cr	CeO <sub>2</sub>	-	International Journal of Hydrogen Energy	10.1016/j.ijhydene.2015.03.044
2015	-	Co <sub>3</sub> O <sub>4</sub>	-	Applied Catalysis A: General	10.1016/j.apcata.2014.10.024
2015	CuO	Fe <sub>2</sub> O <sub>3</sub>	-	Chinese Journal of Catalysis	10.1016/S1872-2067(15)60922-6
2015	Au	Zeolite	-	Catalysis Communications	10.1016/j.catcom.2015.06.018
2015	Pt	CeO <sub>2</sub>	-	Catalysis Today	10.1016/j.cattod.2014.12.038
2015	Au, Cu	CeO <sub>2</sub>	ZrO <sub>2</sub>	Catalysis Today	10.1016/j.cattod.2014.08.035
2015	-	PtO <sub>2</sub>	-	Applied Surface Science	10.1016/j.apsusc.2015.03.108
2015	CuO	CeO <sub>2</sub>	ZrO <sub>2</sub>	Journal of Industrial and Engineering Chemistry	10.1016/j.jiec.2015.06.038
2015	-	MnO <sub>2</sub>	CeO <sub>2</sub>	Applied Catalysis B: Environmental	10.1016/j.apcatb.2014.06.038
2016	Pd	Fe <sub>2</sub> O <sub>3</sub>	-	Journal of Environmental Chemical Engineering	10.1016/j.jece.2016.10.019
2016	-	CeO <sub>2</sub>	ZrO <sub>2</sub>	Applied Catalysis B: Environmental	10.1016/j.apcatb.2016.02.023
2016	Au	Zn <sub>2</sub> SnO <sub>4</sub>	-	Chinese Journal of Catalysis	10.1016/S1872-2067(16)62468-3
2016	-	Co <sub>3</sub> O <sub>4</sub>	-	Catalysis Communications	10.1016/j.catcom.2016.08.020
2016	Au	CeO <sub>2</sub>	-	Applied Catalysis B: Environmental	10.1016/j.apcatb.2016.02.025
2016	Pd	CeO <sub>2</sub>	-	Journal of Molecular Catalysis A: Chemical	10.1016/j.molcata.2016.08.035
2016	-	SiO <sub>2</sub>	Al <sub>2</sub> O <sub>3</sub>	Journal of Molecular Graphics and Modelling	10.1016/j.jmgm.2016.08.005
2016	Ag	SiO <sub>2</sub>	-	Catalysis Today	10.1016/j.cattod.2016.05.033
2016	-	PdO	-	Surface Science	10.1016/j.susc.2015.08.043
2016	-	Co <sub>3</sub> O <sub>4</sub>	-	Applied Catalysis A: General	10.1016/j.apcata.2016.03.027
2016	CuO	TiO <sub>2</sub>	-	Catalysis Communications	10.1016/j.catcom.2016.02.001
2016	Pt	CeO <sub>2</sub>	-	Applied Catalysis B: Environmental	10.1016/j.apcatb.2016.01.056
2016	CuO	MnO <sub>2</sub>	-	Journal of Molecular Catalysis A: Chemical	10.1016/j.molcata.2016.08.024
2016	CuO	Peroskita	-	Applied Clay Science	10.1016/j.clay.2015.08.034
2016	Pd	ZnO	-	Catalysis Today	10.1016/j.cattod.2015.05.021
2016	-	Fe <sub>2</sub> O <sub>3</sub>	-	Chemical Engineering Journal	10.1016/j.cej.2016.04.136
2016	Au	TiO <sub>2</sub>	-	Catalysis Today	10.1016/j.cattod.2015.09.040
2016	Au	Fe <sub>2</sub> O <sub>3</sub>	CeO <sub>2</sub>	Catalysis Today	10.1016/j.cattod.2016.05.059
2016	-	Co <sub>3</sub> O <sub>4</sub>	-	Materials Letters	10.1016/j.matlet.2016.06.108
2016	-	Co <sub>3</sub> O <sub>4</sub>	-	Chinese Journal of Catalysis	10.1016/S1872-2067(15)60969-X
2016	Au	TiO <sub>2</sub>	-	Applied Surface Science	10.1016/j.apsusc.2016.01.285
2016	-	Fe <sub>2</sub> O <sub>3</sub>	-	Journal of Molecular Catalysis A: Chemical	10.1016/j.molcata.2016.01.003
2016	Au	Other	-	Journal of Colloid and Interface Science	10.1016/j.jcis.2016.06.072
2016	Au	LaPO <sub>4</sub>	-	Journal of the Taiwan Institute of Chemical Engineers	10.1016/j.jtice.2016.01.016
2016	Pt	Al <sub>2</sub> O <sub>3</sub>	-	International Journal of Hydrogen Energy	10.1016/j.ijhydene.2016.08.170
2016	Pt	Other	-	Surface Science	10.1016/j.susc.2015.08.024

Table A2. Cont.

Date	Active Metals	Metal Oxide I	Metal Oxide II	Journal	Digital Object Identifier (DOI)
2017	CuO	Nb <sub>2</sub> O <sub>5</sub>	-	Catalysis Communications	10.1016/j.catcom.2017.04.008
2017	Zn, Pt	CeO <sub>2</sub>	-	Applied Catalysis B: Environmental	10.1016/j.apcatb.2017.04.044
2017	Pt, Fe	Fe <sub>2</sub> O <sub>3</sub>	Co <sub>3</sub> O <sub>4</sub>	Chinese Journal of Catalysis	10.1016/S1872-2067(17)62838-9
2017	CuO	MnO <sub>2</sub>	CeO <sub>2</sub>	Catalysis Communications	10.1016/j.catcom.2017.05.016
2017	Pt	MnO <sub>2</sub>	-	Journal of Electroanalytical Chemistry	10.1016/j.jelechem.2016.09.031
2017	Au	LaPO <sub>4</sub>	-	Chinese Journal of Chemical Engineering	10.1016/j.cjche.2017.08.008
2017	Fe, Mn	CeO <sub>2</sub>	-	Catalysis Today	10.1016/j.cattod.2016.11.046
2017	Mn	Co <sub>3</sub> O <sub>4</sub>	-	Solid State Sciences	10.1016/j.solidstatesciences.2017.07.006
2017	Mn	Co <sub>3</sub> O <sub>4</sub>	-	Fuel	10.1016/j.fuel.2017.04.140
2017	Au	CeO <sub>2</sub>	-	Applied Surface Science	10.1016/j.apsusc.2017.04.158
2017	-	MgO	-	Applied Catalysis B: Environmental	10.1016/j.apcatb.2016.11.043
2017	CuO	CeO <sub>2</sub>	Zeolite	Microporous and Mesoporous Materials	10.1016/j.micromeso.2017.02.016
2017	-	Zeolite	-	Applied Catalysis B: Environmental	10.1016/j.apcatb.2017.06.083
2017	Co	ZnO	-	Ceramics International	10.1016/j.ceramint.2017.06.157
2017	Pd	TiO <sub>2</sub>	SnO <sub>2</sub>	Applied Catalysis B: Environmental	10.1016/j.apcatb.2017.02.017
2017	Pd	Fe <sub>2</sub> O <sub>3</sub>	-	Fuel Processing Technology	10.1016/j.fuproc.2017.02.037
2017	CuO	CeO <sub>2</sub>	-	Journal of Power Sources	10.1016/j.jpowsour.2017.01.127
2017	Mn	CeO <sub>2</sub>	-	Applied Catalysis B: Environmental	10.1016/j.apcatb.2017.03.049
2017	Co	Co <sub>3</sub> O <sub>4</sub>	-	Chemical Physics Letters	10.1016/j.cplett.2017.02.085
2017	Au	TiO <sub>2</sub>	-	Catalysis Today	10.1016/j.cattod.2016.05.056
2017	CuO	CeO <sub>2</sub>	-	International Journal of Hydrogen Energy	10.1016/j.ijhydene.2017.02.088
2017	CuO	CeO <sub>2</sub>	-	Journal of Rare Earths	10.1016/j.jre.2017.05.015
2017	Pd	Al <sub>2</sub> O <sub>3</sub>	-	Applied Catalysis B: Environmental	10.1016/j.apcatb.2017.02.038
2017	Pt	TiO <sub>2</sub>	-	Molecular Catalysis	10.1016/j.mcat.2017.01.014
2017	-	CeO <sub>2</sub>	Other	Catalysis Today	10.1016/j.cattod.2017.06.017
2017	-	Al <sub>2</sub> O <sub>3</sub>	SnO <sub>2</sub>	Applied Surface Science	10.1016/j.apsusc.2017.01.058
2017	Ag	Zeolite	-	Fuel	10.1016/j.fuel.2016.10.037
2017	Au	TiO <sub>2</sub>	-	Applied Surface Science	10.1016/j.apsusc.2016.10.076
2017	-	Carbon	-	Molecular Catalysis	10.1016/j.molcata.2016.12.007
2017	Ag	SiO <sub>2</sub>	-	Microporous and Mesoporous Materials	10.1016/j.micromeso.2017.01.016
2017	Pd, Rh	Al <sub>2</sub> O <sub>3</sub>	-	Catalysis Today	10.1016/j.cattod.2016.10.010
2017	Au, Cu	SiO <sub>2</sub>	-	Catalysis Today	10.1016/j.cattod.2016.08.003
2017	Pd	CeO <sub>2</sub>	MnO	Applied Catalysis B: Environmental	10.1016/j.apcatb.2017.01.020
2017	-	CeO <sub>2</sub>	-	Catalysis Today	10.1016/j.cattod.2016.04.016
2017	Pd	Co <sub>3</sub> O <sub>4</sub>	-	Applied Catalysis A: General	10.1016/j.apcata.2016.12.021
2017	Pt	CeO <sub>2</sub>	-	Applied Catalysis A: General	10.1016/j.apcata.2017.08.012
2017	Mn	Co <sub>3</sub> O <sub>4</sub>	-	Solid State Sciences	10.1016/j.solidstatesciences.2017.07.006
2017	Ni	ZrO <sub>2</sub>	-	Applied Catalysis A: General	10.1016/j.apcata.2017.02.001
2018	-	SiO <sub>2</sub>	Co <sub>3</sub> O <sub>4</sub>	Microporous and Mesoporous Materials	10.1016/j.micromeso.2017.07.016
2018	Pt	Fe <sub>2</sub> O <sub>3</sub>	-	Applied Catalysis A: General	10.1016/j.apcata.2018.09.014
2018	Pd	SiO <sub>2</sub>	Al <sub>2</sub> O <sub>3</sub>	Applied Catalysis B: Environmental	10.1016/j.apcatb.2018.06.059
2018	Cu	CeO <sub>2</sub>	-	Catalysis Today	10.1016/j.cattod.2018.10.037
2018	Cu -Ni	CeO <sub>2</sub>	Al <sub>2</sub> O <sub>3</sub>	International Journal of Hydrogen Energy	10.1016/j.ijhydene.2018.12.127
2018	Ru	TiO <sub>2</sub>	ZrO <sub>2</sub>	International Journal of Hydrogen Energy	10.1016/j.ijhydene.2018.10.061
2018	Ni	ZrO <sub>2</sub>	-	International Journal of Hydrogen Energy	10.1016/j.ijhydene.2018.06.173
2018	-	ZrO <sub>2</sub>	-	Applied Catalysis B: Environmental	10.1016/j.apcatb.2018.03.001
2018	Ni	ZrO <sub>2</sub>	-	Applied Catalysis B: Environmental	10.1016/j.apcatb.2018.06.045
2019	Au	TiO <sub>2</sub>	-	International Journal of Hydrogen Energy	10.1016/j.ijhydene.2018.11.050
2019	Cu	Co <sub>3</sub> O <sub>4</sub>	-	Molecular Catalysis	10.1016/j.mcat.2019.01.020
2019	-	Other	-	Applied Catalysis B: Environmental	10.1016/j.apcatb.2018.12.022
2019	Pt	Zeolite	-	Applied Catalysis A: General	10.1016/j.apcata.2018.12.034
2019	Ni	ZrO <sub>2</sub>	-	Applied Catalysis B: Environmental	10.1016/j.apcatb.2018.11.024

## References

- Zhang, K.; Jiang, X. An investigation of fuel variability effect on bio-syngas combustion using uncertainty quantification. *Fuel* **2018**, *220*, 283–295. [CrossRef]
- Renzi, M.; Patuzzi, F.; Baratieri, M. Syngas feed of micro gas turbines with steam injection: Effects on performance, combustion and pollutants formation. *Appl. Energy* **2017**, *206*, 697–707. [CrossRef]
- Rosa, A. Chapter 10—Hydrogen Production. In *Fundamentals of Renewable Energy Processes*, 3rd ed.; Academic Press: Cambridge, MA, USA, 2013; pp. 371–428.
- Mohammed, H.; Al-Othman, A.; Nancarrow, P.; Tawalbeh, M.; El Haj Assad, M. Direct hydrocarbon fuel cells: A promising technology for improving energy efficiency. *Energy* **2019**, *172*, 207–219. [CrossRef]
- Sengodan, S.; Lan, R.; Humphreys, J.; Du, D.; Xu, W.; Wang, H.; Tao, S. Advances in reforming and partial oxidation of hydrocarbons for hydrogen production and fuel cell applications. *Renew. Sustain. Energy Rev.* **2018**, *82*, 761–780. [CrossRef]
- Cifuentes, B.; Hernández, M.; Monsalve, S.; Cobo, M. Hydrogen production by steam reforming of ethanol on a RhPt/CeO<sub>2</sub>/SiO<sub>2</sub> catalyst: Synergistic effect of the Si:Ce ratio on the catalyst performance. *Appl. Catal. A Gen.* **2016**, *523*, 283–293. [CrossRef]

7. Xie, Y.; Wu, J.; Jing, G.; Zhang, H.; Zeng, S.; Tian, X.; Zou, X.; Wen, J.; Su, H.; Zhong, C.J.; et al. Structural origin of high catalytic activity for preferential CO oxidation over CuO/CeO<sub>2</sub> nanocatalysts with different shapes. *Appl. Catal. B Environ.* **2018**, *239*, 665–676. [[CrossRef](#)]
8. Kou, T.; Si, C.; Gao, Y.; Frenzel, J.; Wang, H.; Yan, X.; Bai, Q.; Eggeler, G.; Zhang, Z. Large-scale synthesis and catalytic activity of nanoporous Cu-O system towards CO oxidation. *RSC Adv.* **2014**, *4*, 65004–65011. [[CrossRef](#)]
9. Kou, T.; Si, C.; Pinto, J.; Ma, C.; Zhang, Z. Dealloying assisted high-yield growth of surfactant-free (110) highly active Cu-doped CeO<sub>2</sub> nanowires for low-temperature CO oxidation. *Nanoscale* **2017**, *9*, 8007–8014. [[CrossRef](#)]
10. Ashraf, M.A.; Ercolino, G.; Specchia, S.; Specchia, V. Final step for CO syngas clean-up: Comparison between CO-PROX and CO-SMET processes. *Int. J. Hydrogen Energy* **2014**, *39*, 18109–18119. [[CrossRef](#)]
11. Rossetti, I.; Compagnoni, M.; Torli, M. Process simulation and optimization of H<sub>2</sub> production from ethanol steam reforming and its use in fuel cells. 2. Process analysis and optimization. *Chem. Eng. J.* **2015**, *281*, 1036–1044. [[CrossRef](#)]
12. Gubán, D.; Tompos, A.; Bakos, I.; Vass, Á.; Pászti, Z.; Szabó, E.G.; Sajó, I.E.; Borbáth, I. Preparation of CO-tolerant anode electrocatalysts for polymer electrolyte membrane fuel cells. *Int. J. Hydrogen Energy* **2017**, *42*, 13741–13753. [[CrossRef](#)]
13. Narayanan, H.; Basu, S. Regeneration of CO poisoned Pt black anode catalyst in PEMFC using break-in procedure and KMnO<sub>4</sub> solution. *Int. J. Hydrogen Energy* **2017**, *42*, 23814–23820. [[CrossRef](#)]
14. Devrim, Y.; Albostan, A.; Devrim, H. Experimental investigation of CO tolerance in high temperature PEM fuel cells. *Int. J. Hydrogen Energy* **2018**, *43*, 18672–18681. [[CrossRef](#)]
15. Kugai, J.; Fox, E.B.; Song, C. Kinetic characteristics of oxygen-enhanced water gas shift on CeO<sub>2</sub>-supported Pt–Cu and Pd–Cu bimetallic catalysts. *Appl. Catal. A Gen.* **2015**, *497*, 31–41. [[CrossRef](#)]
16. Xu, G.; Zhang, Z.G. Preferential CO oxidation on Ru/Al<sub>2</sub>O<sub>3</sub> catalyst: An investigation by considering the simultaneously involved methanation. *J. Power Sources* **2006**, *157*, 64–77. [[CrossRef](#)]
17. Reina, T.R.; Ivanova, S.; Laguna, O.H.; Centeno, M.A.; Odriozola, J.A. WGS and CO-PrOx reactions using gold promoted copper-ceria catalysts: “bulk CuO–CeO<sub>2</sub> vs. CuO–CeO<sub>2</sub>/Al<sub>2</sub>O<sub>3</sub> with low mixed oxide content”. *Appl. Catal. B Environ.* **2016**, *197*, 67–72. [[CrossRef](#)]
18. Wang, F.; Zhang, J.-C.; Li, W.-Z.; Chen, B.-H. Coke-resistant Au–Ni/MgAl<sub>2</sub>O<sub>4</sub> catalyst for direct methanation of syngas. *J. Energy Chem.* **2019**, *39*, 198–207. [[CrossRef](#)]
19. Reina, T.R.R.; Ivanova, S.; Centeno, M.A.A.; Odriozola, J.A.A. Catalytic screening of Au/CeO<sub>2</sub>-MO<sub>x</sub>/Al<sub>2</sub>O<sub>3</sub> (M = La, Ni, Cu, Fe, Cr, Y) in the CO-PrOx reaction. *Int. J. Hydrogen Energy* **2015**, *40*, 1782–1788. [[CrossRef](#)]
20. Cifuentes, B.; Bustamante, F.; Conesa, J.A.; Córdoba, L.F.; Cobo, M. Fuel-cell grade hydrogen production by coupling steam reforming of ethanol and carbon monoxide removal. *Int. J. Hydrogen Energy* **2018**, *43*, 17216–17229. [[CrossRef](#)]
21. Yao, X.; Gao, F.; Dong, L. The application of incorporation model in  $\gamma$ -Al<sub>2</sub>O<sub>3</sub>-supported single and dual metal oxide catalysts: A review. *Cuihua Xuebao/Chin. J. Catal.* **2013**, *34*, 1975–1985. [[CrossRef](#)]
22. MacIel, C.G.; Profeti, L.P.R.; Assaf, E.M.; Assaf, J.M. Hydrogen purification for fuel cell using CuO/CeO<sub>2</sub>-Al<sub>2</sub>O<sub>3</sub> catalyst. *J. Power Sources* **2011**, *196*, 747–753. [[CrossRef](#)]
23. Águila, G.; Gracia, F.; Araya, P. CuO and CeO<sub>2</sub> catalysts supported on Al<sub>2</sub>O<sub>3</sub>, ZrO<sub>2</sub>, and SiO<sub>2</sub> in the oxidation of CO at low temperature. *Appl. Catal. A Gen.* **2008**, *343*, 16–24. [[CrossRef](#)]
24. Zhao, Z.; Lin, X.; Jin, R.; Dai, Y.; Wang, G. High catalytic activity in CO PROX reaction of low cobalt-oxide loading catalysts supported on nano-particulate CeO<sub>2</sub>-ZrO<sub>2</sub> oxides. *Catal. Commun.* **2011**, *12*, 1448–1451. [[CrossRef](#)]
25. Moretti, E.; Rodríguez-Aguado, E.; Molina, A.I.; Rodríguez-Castellón, E.; Talon, A.; Storaro, L. Sustainable photo-assisted CO oxidation in H<sub>2</sub>-rich stream by simulated solar light response of Au nanoparticles supported on TiO<sub>2</sub>. *Catal. Today* **2018**, *304*, 135–142. [[CrossRef](#)]
26. Li, S.; Tang, H.; Gong, D.; Ma, Z.; Liu, Y. Loading Ni/La<sub>2</sub>O<sub>3</sub> on SiO<sub>2</sub> for CO methanation from syngas. *Catal. Today* **2017**, *297*, 298–307. [[CrossRef](#)]
27. Liu, S.; Wu, X.; Weng, D.; Ran, R. Ceria-based catalysts for soot oxidation: A review. *J. Rare Earths* **2015**, *33*, 567–590. [[CrossRef](#)]
28. Martínez, L.M.; Laguna, O.H.; López-Cartes, C.; Centeno, M.A. Synthesis and characterization of Rh/MnO<sub>2</sub>-CeO<sub>2</sub>/Al<sub>2</sub>O<sub>3</sub> catalysts for CO-PrOx reaction. *Mol. Catal.* **2017**, *440*, 9–18. [[CrossRef](#)]

29. Gamboa-Rosales, N.K.; Ayastuy, J.L.; González-Marcos, M.P.; Gutiérrez-Ortiz, M.A. Effect of Au promoter in CuO/CeO<sub>2</sub> catalysts for the oxygen-assisted WGS reaction. *Catal. Today* **2011**, *176*, 63–71. [[CrossRef](#)]
30. Destro, P.; Marras, S.; Manna, L.; Colombo, M.; Zanchet, D. AuCu alloy nanoparticles supported on SiO<sub>2</sub>: Impact of redox pretreatments in the catalyst performance in CO oxidation. *Catal. Today* **2017**, *282*, 105–110. [[CrossRef](#)]
31. Destro, P.; Kokumai, T.M.; Scarpellini, A.; Pasquale, L.; Manna, L.; Colombo, M.; Zanchet, D. The Crucial Role of the Support in the Transformations of Bimetallic Nanoparticles and Catalytic Performance. *ACS Catal.* **2017**, *8*, 1031–1037. [[CrossRef](#)]
32. Ayastuy, J.L.; Gurbani, A.; Gutiérrez-Ortiz, M.A. Effect of calcination temperature on catalytic properties of Au/Fe<sub>2</sub>O<sub>3</sub> catalysts in CO-PROX. *Int. J. Hydrogen Energy* **2016**, *41*, 19546–19555. [[CrossRef](#)]
33. Lakshmanan, P.; Park, E. Preferential CO Oxidation in H<sub>2</sub> over Au/La<sub>2</sub>O<sub>3</sub>/Al<sub>2</sub>O<sub>3</sub> Catalysts: The Effect of the Catalyst Reduction Method. *Catalysts* **2018**, *8*, 183–193. [[CrossRef](#)]
34. Córdoba, L.F.; Martínez-Hernández, A. Preferential oxidation of CO in excess of hydrogen over Au/CeO<sub>2</sub>-ZrO<sub>2</sub> catalysts. *Int. J. Hydrogen Energy* **2015**, *40*, 16192–16201. [[CrossRef](#)]
35. Arévalo, J.D.; Martínez-Hernández, Á.; Vargas, J.C.; Córdoba, L.F. Hydrogen Production and Purification by Bioethanol Steam Reforming and Preferential Oxidation of CO. *Tecciencia* **2018**, *13*, 55–64.
36. Chen, Z.; Pursell, C.J.; Chandler, B.D.; Saavedra, J.; Whittaker, T.; Rioux, R.M. Controlling activity and selectivity using water in the Au-catalysed preferential oxidation of CO in H<sub>2</sub>. *Nat. Chem.* **2016**, *8*, 584–589.
37. Dasireddy, V.D.B.C.; Valand, J.; Likozar, B. PROX reaction of CO in H<sub>2</sub>/H<sub>2</sub>O/CO<sub>2</sub> Water–Gas Shift (WGS) feedstocks over Cu–Mn/Al<sub>2</sub>O<sub>3</sub> and Cu–Ni/Al<sub>2</sub>O<sub>3</sub> catalysts for fuel cell applications. *Renew. Energy* **2018**, *116*, 75–87. [[CrossRef](#)]
38. Zhan, W.; Wang, J.; Wang, H.; Zhang, J.; Liu, X.; Zhang, P.; Chi, M.; Guo, Y.; Guo, Y.; Lu, G.; et al. Crystal Structural Effect of AuCu Alloy Nanoparticles on Catalytic CO Oxidation. *J. Am. Chem. Soc.* **2017**, *139*, 8846–8854. [[CrossRef](#)]
39. Reina, T.R.; Megías-Sayago, C.; Florez, A.P.; Ivanova, S.; Centeno, M.Á.; Odriozola, J.A. H<sub>2</sub> oxidation as criterion for PrOx catalyst selection: Examples based on Au–CoOx-supported systems. *J. Catal.* **2015**, *326*, 161–171. [[CrossRef](#)]
40. Yung, M.M.; Zhao, Z.; Woods, M.P.; Ozkan, U.S. Preferential oxidation of carbon monoxide on CoOx/ZrO<sub>2</sub>. *J. Mol. Catal. A Chem.* **2008**, *279*, 1–9. [[CrossRef](#)]
41. Fonseca, J.D.; Ferreira, H.S.; Bion, N.; Pirault-Roy, L.; do Carmo Rangel, M.; Duprez, D.; Epron, F. Cooperative effect between copper and gold on ceria for CO-PROX reaction. *Catal. Today* **2012**, *180*, 34–41. [[CrossRef](#)]
42. Proaño, L.; Tello, E.; Arellano-Trevino, M.A.; Wang, S.; Farrauto, R.J.; Cobo, M. In-Situ DRIFTS study of two-step CO<sub>2</sub> capture and catalytic methanation over Ru, “Na<sub>2</sub>O”/Al<sub>2</sub>O<sub>3</sub> Dual Functional Material. *Appl. Surf. Sci.* **2019**, *479*, 25–30. [[CrossRef](#)]
43. Jhalani, A.; Schmidt, L.D. Preferential CO oxidation in the presence of H<sub>2</sub>, H<sub>2</sub>O and CO<sub>2</sub> at short contact-times. *Catal. Lett.* **2005**, *104*, 103–110. [[CrossRef](#)]
44. Tanaka, K.I.; He, H.; Shou, M.; Shi, X. Mechanism of highly selective low temperature PROX reaction of CO in H<sub>2</sub>: Oxidation of CO via HCOO with OH. *Catal. Today* **2011**, *175*, 467–470. [[CrossRef](#)]
45. Wang, F.; Zhang, L.; Zhu, J.; Han, B.; Zhao, L.; Yu, H.; Deng, Z.; Shi, W. Study on different CeO<sub>2</sub> structure stability during ethanol steam reforming reaction over Ir/CeO<sub>2</sub> nanocatalysts. *Appl. Catal. A Gen.* **2018**, *564*, 226–233. [[CrossRef](#)]
46. Divins, N.J.; Casanovas, A.; Xu, W.; Senanayake, S.D.; Wiater, D.; Trovarelli, A.; Llorca, J. The influence of nano-architected CeOx supports in RhPd/CeO<sub>2</sub> for the catalytic ethanol steam reforming reaction. *Catal. Today* **2015**, *253*, 99–105. [[CrossRef](#)]
47. Li, X.; Fang, S.S.; Teo, J.; Foo, Y.L.; Borgna, A.; Lin, M.; Zhong, Z. Activation and deactivation of Au–Cu/SBA-15 catalyst for preferential oxidation of CO in H<sub>2</sub>-Rich Gas. *ACS Catal.* **2012**, *2*, 360–369. [[CrossRef](#)]
48. Laguna, O.H.; Hernández, W.Y.; Arzamendi, G.; Gandía, L.M.; Centeno, M.A.; Odriozola, J.A. Gold supported on CuOx/CeO<sub>2</sub> catalyst for the purification of hydrogen by the CO preferential oxidation reaction (PROX). *Fuel* **2014**, *118*, 176–185. [[CrossRef](#)]
49. Redina, E.A.; Greish, A.A.; Mishin, I.V.; Kapustin, G.I.; Tkachenko, O.P.; Kirichenko, O.A.; Kustov, L.M. Selective oxidation of ethanol to acetaldehyde over Au–Cu catalysts prepared by a redox method. *Catal. Today* **2015**, *241*, 246–254. [[CrossRef](#)]

50. Wang, J.; Zhong, L.; Lu, J.; Chen, R.; Lei, Y.; Chen, K.; Han, C.; He, S.; Wan, G.; Luo, Y. A solvent-free method to rapidly synthesize CuO–CeO<sub>2</sub> catalysts to enhance their CO preferential oxidation: Effects of Cu loading and calcination temperature. *Mol. Catal.* **2017**, *443*, 241–252. [[CrossRef](#)]
51. Wang, X.; Rodriguez, J.A.; Hanson, J.C.; Gamarra, D.; Martínez-Arias, A.; Fernández-García, M. In Situ Studies of the Active Sites for the Water Gas Shift Reaction over Cu–CeO<sub>2</sub> Catalysts: Complex Interaction between Metallic Copper and Oxygen Vacancies of Ceria. *J. Phys. Chem. B* **2006**, *110*, 428–434. [[CrossRef](#)]
52. Wang, F.; Büchel, R.; Savitsky, A.; Zalibera, M.; Widmann, D.; Pratsinis, S.E.; Lubitz, W.; Schüth, F. In Situ EPR Study of the Redox Properties of CuO–CeO<sub>2</sub> Catalysts for Preferential CO Oxidation (PROX). *ACS Catal.* **2016**, *6*, 3520–3530. [[CrossRef](#)]
53. Mallát, T.; Szabó, S.; Petró, J.; Mendioroz, S.; Folgado, M.A. Real and apparent dispersion of carbon supported palladium-cobalt catalysts. *Appl. Catal.* **1989**, *53*, 29–40. [[CrossRef](#)]
54. Barbato, P.S.; Colussi, S.; Di Benedetto, A.; Landi, G.; Lisi, L.; Llorca, J.; Trovarelli, A. Origin of High Activity and Selectivity of CuO/CeO<sub>2</sub> Catalysts Prepared by Solution Combustion Synthesis in CO-PROX Reaction. *J. Phys. Chem. C* **2016**, *120*, 13039–13048. [[CrossRef](#)]
55. Schüth, F.; Ward, M.D.; Buriak, J.M. Common Pitfalls of Catalysis Manuscripts Submitted to Chemistry of Materials. *Chem. Mater.* **2018**, *30*, 3599–3600. [[CrossRef](#)]
56. Cifuentes, B.; Valero, M.; Conesa, J.; Cobo, M. Hydrogen Production by Steam Reforming of Ethanol on Rh-Pt Catalysts: Influence of CeO<sub>2</sub>, ZrO<sub>2</sub>, and La<sub>2</sub>O<sub>3</sub> as Supports. *Catalysts* **2015**, *5*, 1872–1896. [[CrossRef](#)]
57. Nagaraja, B.M.; Padmasri, A.H.; Raju, B.D.; Rao, K.S.R. Vapor phase selective hydrogenation of furfural to furfuryl alcohol over Cu-MgO coprecipitated catalysts. *J. Mol. Catal. A Chem.* **2007**, *265*, 90–97. [[CrossRef](#)]
58. Li, J.; Zhan, Y.; Lin, X.; Zheng, Q. Influence of Calcination Temperature on Properties of Au/Fe<sub>2</sub>O<sub>3</sub> Catalysts for Low Temperature Water Gas Shift Reaction. *Acta Phys.-Chim. Sin.* **2008**, *24*, 932–938. [[CrossRef](#)]
59. Liu, F.; Xiao, Y.; Sun, X.; Qin, G.; Song, X.; Liu, Y. Synergistic catalysis over hollow CeO<sub>2</sub>–CaO–ZrO<sub>2</sub> nanostructure for polycarbonate methanolysis with methanol. *Chem. Eng. J.* **2019**, *369*, 205–214. [[CrossRef](#)]
60. Chen, W.; Ran, R.; Weng, D.; Wu, X.; Zhong, J.; Han, S. Influence of morphology on basicity of CeO<sub>2</sub> and its use in 2-chloroethyl ethyl sulfide degradation. *J. Rare Earths* **2017**, *35*, 970–976. [[CrossRef](#)]
61. Malik, A.S.; Zaman, S.F.; Al-Zahrani, A.A.; Daous, M.A.; Driss, H.; Petrov, L.A. Selective hydrogenation of CO<sub>2</sub> to CH<sub>3</sub>OH and in-depth DRIFT analysis for PdZn/ZrO<sub>2</sub> and CaPdZn/ZrO<sub>2</sub> catalysts. *Catal. Today* **2019**, in press. [[CrossRef](#)]
62. Zhou, W.; Ma, Z.; Guo, S.; Wang, M.; Wang, J.; Xia, M.; Jia, L.; Hou, B.; Li, D.; Zhao, Y. Comparative study of CO adsorption on zirconia polymorphs with DRIFT and transmission FT-IR spectroscopy. *Appl. Surf. Sci.* **2018**, *427*, 867–873. [[CrossRef](#)]
63. Agarwal, S.; Mojet, B.L.; Lefferts, L.; Datye, A.K. Ceria Nanoshapes-Structural and Catalytic Properties. In *Catalysis by Materials with Well-Defined Structures*; Elsevier: Amsterdam, The Netherlands, 2015; pp. 31–70.
64. Leba, A.; Davran-Candan, T.; Önsan, Z.I.; Yildirim, R. DRIFTS study of selective CO oxidation over Au/γAl<sub>2</sub>O<sub>3</sub> catalyst. *Catal. Commun.* **2012**, *29*, 6–10. [[CrossRef](#)]
65. Fernández-García, S.; Collins, S.E.; Tinoco, M.; Hungría, A.B.; Calvino, J.J.; Cauqui, M.A.; Chen, X. Influence of {111} nanofaceting on the dynamics of CO adsorption and oxidation over Au supported on CeO<sub>2</sub> nanocubes: An operando DRIFT insight. *Catal. Today* **2019**, *336*, 90–98. [[CrossRef](#)]
66. Gamarra, D.; Martínez-Arias, A. Preferential oxidation of CO in rich H<sub>2</sub> over CuO/CeO<sub>2</sub>: Operando-DRIFTS analysis of deactivating effect of CO<sub>2</sub> and H<sub>2</sub>O. *J. Catal.* **2009**, *263*, 189–195. [[CrossRef](#)]
67. Moretti, E.; Lenarda, M.; Storaro, L.; Talon, A.; Frattini, R.; Polizzi, S.; Rodríguez-Castellón, E.; Jiménez-López, A. Catalytic purification of hydrogen streams by PROX on Cu supported on an organized mesoporous ceria-modified alumina. *Appl. Catal. B Environ.* **2007**, *72*, 149–156. [[CrossRef](#)]
68. Polster, C.S.; Nair, H.; Baertsch, C.D. Study of active sites and mechanism responsible for highly selective CO oxidation in H<sub>2</sub> rich atmospheres on a mixed Cu and Ce oxide catalyst. *J. Catal.* **2009**, *266*, 308–319. [[CrossRef](#)]
69. Suzuki, Y.; Hayakawa, K.; Fukuhara, C.; Watanabe, R.; Kawasaki, W. A novel nickel-based structured catalyst for CO<sub>2</sub> methanation: A honeycomb-type Ni/CeO<sub>2</sub> catalyst to transform greenhouse gas into useful resources. *Appl. Catal. A Gen.* **2016**, *532*, 12–18.
70. Le, T.A.; Kim, M.S.; Lee, S.H.; Kim, T.W.; Park, E.D. CO and CO<sub>2</sub> methanation over supported Ni catalysts. *Catal. Today* **2017**, *293–294*, 89–96. [[CrossRef](#)]

71. Sahoo, D.R.; Vajpai, S.; Patel, S.; Pant, K.K. Kinetic modeling of steam reforming of ethanol for the production of hydrogen over Co/Al<sub>2</sub>O<sub>3</sub> catalyst. *Chem. Eng. J.* **2007**, *125*, 139–147. [[CrossRef](#)]
72. Cifuentes, B.; Bustamante, F.; Cobo, M. Data for: Single and dual metal oxides as promising supports for carbon monoxide removal from an actual syngas. *Mendeley Datasets* **2019**, 1–10. [[CrossRef](#)]



© 2019 by the authors. Licensee MDPI, Basel, Switzerland. This article is an open access article distributed under the terms and conditions of the Creative Commons Attribution (CC BY) license (<http://creativecommons.org/licenses/by/4.0/>).